

DISCRETE ELEMENT SIMULATIONS OF POWDER SPREADING IN  
ADDITIVE MANUFACTURING

by

Parth Amrapurkar

A thesis submitted to the faculty of  
The University of North Carolina at Charlotte  
in partial fulfillment of the requirements  
for the degree of Master of Science in  
Mechanical Engineering

Charlotte

2020

Approved by:

---

Dr. Harish Cherukuri

---

Dr. Jun Xu

---

Dr. Brigid Mullany



## ABSTRACT

PARTH AMRAPURKAR. Discrete Element Simulations of Powder Spreading in Additive Manufacturing. (Under the direction of DR. HARISH CHERUKURI)

Powder spreading plays a critical role in the quality of parts produced with selective laser sintering (SLS). Some of the important parameters that influence the quality of the powder bed are the powder particle size and distribution, blade speed, blade - bed gap. In this work, the discrete element method is used to study the effect of these parameters on the quality of the powder bed. The interaction between the particles is modelled using Hertz-Mindlin with JKR contact model. The powder bed quality is quantified in the terms of mass flow rate (MFR) and packing density (PD) of powder. It is widely reported in the literature that increasing the packing density has the effect of reducing defects in the finished product. With the help of these quantities various factors affecting the powdered bed quality have been studied: cohesiveness of the particles, coefficient of restitution (COR), powder particle size and distribution, blade speed and gap. The results obtained from this study indicate that the powder particle size distribution is one of the major factor affecting the bed quality and as the blade - bed gap increases and blade speed decreases packing density increases. The blade - bed gap has no impact on MFR of the powder and cohesiveness has a wider impact on PD with smaller particle diameter.

DEDICATION

To my parents,

Mr. Satish Vasantao Amrapurkar and Mrs. Medha Satish Amrapurkar  
without whom none of my success would be possible.

## ACKNOWLEDGEMENTS

I would like to express my sincere gratitude to my advisor Dr. Harish Cherukuri for the continuous support during my time at UNC Charlotte. His patience, motivation and guidance helped me during the entire period of research and writing of this thesis which would have not been possible without him. I would also like to thank Dr. Jun Xu and Dr. Brigid Mullany for serving on my thesis committee and for their valuable feedback.

I would like to thank my dearest friends Amey Mankar, Aditya Sonwane, Manoj Deshpande and Saloni Gupta for their constant support throughout my journey. I am extremely grateful to my colleagues Dhanooj, Nishat and my fellow lab members for their constructive critique and technical advice. Finally, I would like to extend my sincere thanks to faculty and staff from the mechanical engineering department of UNC Charlotte who helped me complete my master's degree.

## TABLE OF CONTENTS

LIST OF TABLES	viii
LIST OF FIGURES	ix
LIST OF ABBREVIATIONS	xi
CHAPTER 1: INTRODUCTION	1
1.1. Literature Review	2
1.2. Objectives of the thesis	4
1.3. Organization of the Thesis	4
CHAPTER 2: THE DISCRETE ELEMENT METHOD	5
CHAPTER 3: DEM IN EDEM	9
3.1. DEM Simulation in EDEM	9
3.2. Contact Models	12
3.2.1. Hertz-Mindlin contact model in EDEM	14
3.2.2. Hertz-Mindlin with JKR Cohesion	17
CHAPTER 4: SIMULATION SETUP IN EDEM	20
4.1. Material Properties	21
4.2. Parametric Study	23
CHAPTER 5: RESULTS AND DISCUSSION	24
5.1. Mass flow rate (MFR)	24
5.1.1. Effect of mass flow rate on gap size for different speeds	26
5.1.2. Study of COR on mass flow rate	27
5.1.3. Study of particle size on mass flow rate	28

	vii
5.1.4. Effect of surface energy on mass flow rate	29
5.2. Packing Density	30
5.2.1. Effect of gap on PD for different gap sizes and velocities	31
5.2.2. Packing density trend with change in COR	34
5.2.3. Change in packing density for different size particles	36
5.2.4. Surface energy and packing density	37
5.2.5. Particle size distribution and Packing density	38
5.3. Angle of repose study	40
5.3.1. Angle of repose and cohesion	41
5.3.2. Effect of gap and blade speed with angle of repose	42
CHAPTER 6: CONCLUSIONS AND RECOMMENDATIONS FOR FUTURE WORK	44
6.1. Conclusions	44
6.2. Recommendations for future work	45
REFERENCES	47

## LIST OF TABLES

TABLE 4.1: Material Properties - Stainless Steel.	21
TABLE 4.2: Material and Process Parameters.	23

## LIST OF FIGURES

FIGURE 1.1: SLM Process.	2
FIGURE 2.1: Hard and soft sphere contacts.	6
FIGURE 2.2: DEM Calculation Sequence.	8
FIGURE 3.1: Simulation / Calculation Sequence in EDEM™ [1].	11
FIGURE 3.2: Dynamic Factory in EDEM.	12
FIGURE 3.3: Static Factory at two time steps.	13
FIGURE 3.4: Hertz-Mindlin Contact Model [2].	15
FIGURE 4.1: Simulation Setup.	20
FIGURE 4.2: Simulation setup (Accumulation & Spreading).	22
FIGURE 5.1: Mass flow rate (MFR) calculation setup.	25
FIGURE 5.2: Mass flow rate (MFR) against Gap/ $D$ and different velocities.	26
FIGURE 5.3: Mass flow rate (MFR) against Gap/ $D$ and different velocities and COR.	27
FIGURE 5.4: Mass flow rate (MFR) against particle diameter $D$ .	28
FIGURE 5.5: Mass flow rate (MFR) against surface energy.	29
FIGURE 5.6: Packing density (PD) setup.	31
FIGURE 5.7: Packing density (PD) against Gap/ $D$ and different velocities.	31
FIGURE 5.8: Particle velocities after spreading for blade speed 0.05 m/s.	33
FIGURE 5.9: Particle velocities after spreading for blade speed 0.16 m/s.	33
FIGURE 5.10: Packing density (PD) against Gap/ $D$ and different velocities and COR.	34

FIGURE 5.11: Powdered bed for different Gap size.	35
FIGURE 5.12: Packing density (PD) against particle diameter $D$ .	36
FIGURE 5.13: Packing density (PD) against surface energy.	37
FIGURE 5.14: Packing density (PD) against capped and uncapped normal distribution.	39
FIGURE 5.15: Capped normal distribution of particle diameter $D$ .	40
FIGURE 5.16: Angle of repose (AOR) setup.	41
FIGURE 5.17: Angle of repose (AOR) with and without cohesion.	41
FIGURE 5.18: Angle of repose (AOR) against Gap/ $D$ and different velocities.	42

## LIST OF ABBREVIATIONS

$\beta$	Ratio with COR
$\delta_c$	Critical gap
$\delta_n$	Normal overlap
$\delta_t$	Tangential overlap
$\gamma$	Surface energy
$\mu_r$	Rolling friction coefficient
$\mu_s$	Static friction coefficient
$\nu$	Poisson's ratio
$\rho$	Material density
$D$	Particle diameter
$E^*$	Equivalent Young's modulus
$F_n^d$	Normal damping force
$F_t^d$	Tangential damping force
$F_n$	Normal spring force
$F_t$	Tangential spring force
$F_{JKR}$	Cohesion force
$F_{nor}$	Normal contact force
$F_{pullout}$	Pullout force
$F_{tan}$	Tangential contact force

$G^*$	Equivalent shear modulus
$l$	Length of cylinder sensor in EDEM™
$m^*$	Equivalent mass
$m_a$	Mass of particle a
$m_b$	Mass of particle b
$R^*$	Equivalent Radius
$S_n$	Normal spring stiffness
$S_t$	Tangential spring stiffness
$v_n^{rel}$	Normal relative velocity
$v_t^{rel}$	Tangential relative velocity
AOR	Angle of Repose
COR	Coefficient of Restitution
DEM	Discrete Element Method
FDM	Fused Deposition Modelling
FEM	Finite Element Method
JKR	Johnson, Kendall and Roberts
MFR	Mass Flow Rate
PD	Packing Density
SLA	Stereo - Lithography
SLS	Selective Laser Sintering

## CHAPTER 1: INTRODUCTION

Additive manufacturing is an innovative and new approach to manufacture components with intricate shapes and features. Additive manufacturing uses polymers as well as metals for manufacturing. Hideo Kodama of Nagoya Municipal Industrial Research Institute is usually credited for the initial development of Additive Manufacturing [3]. He developed a rapid prototyping machine which used a layer-by-layer approach to print a solid part. This technique known as the fused deposition method (FDM) uses polymer in the form of filaments and in SLA or stereo-lithography resins are used to 3D print the components. With new developments in 3D printing and technological advancements, metallic powders are also being used to print metal parts. Techniques in metal additive manufacturing are selective laser sintering (SLS), selective laser melting (SLM), and binder jetting to name a few. The SLS method is patented by Beaman and Deckard from University of Texas Austin in 1988 [4].

Powder Spreading is the first process in selective laser sintering. In schematic 1.1, SLS process is described. The process consist of a blade or spreader which is used to spread the powder. After the powder is spread, a laser is used to fuse the powder such that it satisfies the shape of required component. The powder is spread again on the fused metal for next layer. This layer by layer procss is continued to produce the desired component. The quality of the product manufactured using SLS depends on how the powder is spread and the bed quality [5]. Generally, the bed quality is quantified using the porosity which is affected by many parameters. These include the angle of repose (AOR), blade speed, coefficient of friction between blade and particle and also between particles, coefficient of restitution (COR), particle size and distribution, and cohesion (surface energy) ( $\gamma$ ) between particles [6].

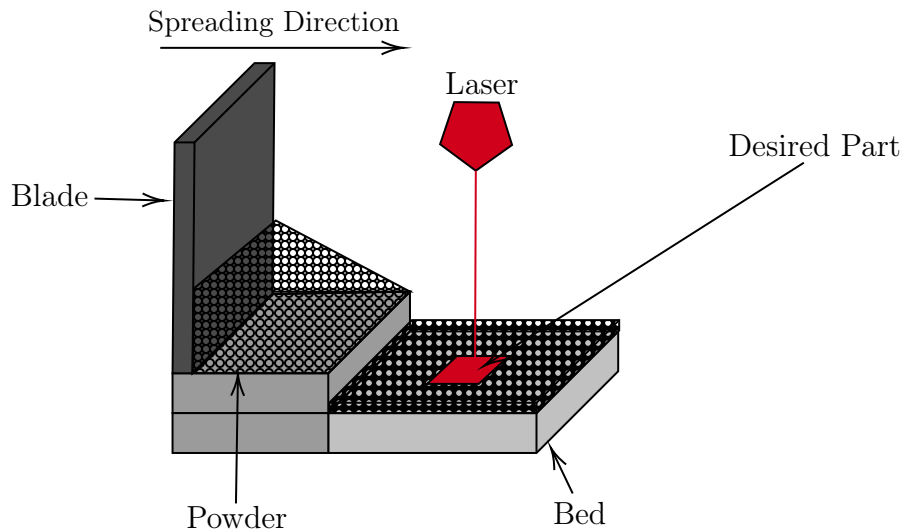


Figure 1.1: Selective Laser Sintering Process Layout.

## 1.1 Literature Review

The effect of various process and powder parameters on the powder bed quality can be studied computationally or experimentally. Since there are a number of parameters, computational methods are preferred over experiments due to low cost and flexibility. However, for reliable predictions, the computational models must be calibrated and validated first using experiments. Once the computational models are validated, various parametric studies can be carried out to study the relationship between process parameters and the powder bed quality.

Although both the Finite Element Method (FEM) or the Discrete Element Method (DEM) are available for modeling purposes, the Discrete Element Method is the more commonly used method for modelling powder spreading problem [7]. While FEM uses continuum mechanics concepts, DEM is particle-based with interactions between particles being taken into account using contact models. Cundall introduced DEM with application in geomechanics in mind. However, later, it was modified and developed for other applications [8].

Many authors have applied DEM to study powder spreading. For example, Parteli et al. [9] studied the blade speed and its effects on the powder bed quality by using a

roller spreader and concluded that if the roller spreader has high translational velocity, the bed quality obtained is low. The bed quality in this study was quantified in terms of space occupied by the powder on bed after spreading. Nan et al. [10] studied the jamming of the particles between the blade and the bed. Nan et al. in [10, 11] also studied shear band formation in front of the blade and its effects on powder spreading and the powdered bed quality. They concluded that particle jamming occurs when the blade - bed gap is significantly small - below  $1.5D$  size. This study included particles of different sizes with diameter in different range and non spherical shapes. Another study, performed by Chen [5], focuses on the model calibration by studying the angle of repose with the help of experiments. In addition, they also studied the effect of coefficient of friction on mass flow rate and angle of repose. In the study performed by Chen in [12], it was observed that the powder bed quality impacts the number of pores and the surface finish of the finished product. [13], DEM simulations of powder scraping process focused on dynamic angle of repose and volume fraction of powder on the bed . The work performed by Jeremy in [14] elaborates on application of discrete element method (DEM) for the study of powder flowability and its variation with material properties.

From the literature survey, it can be inferred that final product quality in metal additive manufacturing process in terms of pores and surface finish depends on powder spreading process. The spreading process is affected by the process parameters. How well the powder is spread can be defined by the powder mass flow rate and the space occupied by the particles on the bed. Studies by Chen et al. [5] and Nan et al. [11] focus on mass flow rate of the powder and angle of repose. Studying the powder packing on the spreaded bed along with the mass flow rate would give a clearer understanding of the overall spreading process. Therefore, the aim of this thesis is to analyze how the process parameters affect these two quantities. Furthermore, the EDEM™ software package provided by DEM Solutions, Edinburgh, UK, is used for the

computational models.

## 1.2 Objectives of the thesis

The objective of this work are as follows:

- To develop a 3D model of powder spreading process with a spreader blade and manufacturing bed using DEM and appropriate contact models that capture various physical phenomena that affect the interactions between particles,
- To develop a quantitative measure of powder bed quality,
- To study parameters such as particle size, blade shape, blade-bed gap, blade speed and their effects on the quality of the powdered bed.

## 1.3 Organization of the Thesis

The rest of the thesis is organized as follows. In Chapters 2 and 3, the discrete element method, its implementation in EDEM<sup>TM</sup> along with the contact models used for the study, and the numerical schemes used to solve the DEM equations are discussed. Chapter 4 briefs on how the powder bed is modelled along with the material properties used and the objectives. The effect of various parameters such as the blade-bed gap, blade speed, coefficient of restitution (COR), surface energy etc on the powdered bed quality in terms of mass flow rate (MFR) and packing density (PD) is studied in Chapter 5. Lastly, Chapter 6 summarizes the conclusions and recommendations for future work.

## CHAPTER 2: THE DISCRETE ELEMENT METHOD

In computational mechanics, there are two different types of modelling approaches, continuum and discrete modelling. The continuum modelling approach is based on the assumption that the domain of model is continuous. For modeling powder materials, an approach that takes into consideration the behaviour of each particle is more suitable. The Discrete Element Method (DEM) is a particle-based method that is commonly used for this purpose. In DEM, each particle is considered as a separate body and its interaction with other particles is studied through contact models. Since each particle has the potential to come into contact with several particles, the method is computationally intensive. For this method, the method did not find wide use until recently. However, with the advances in computing power along with the advent of GPU computing, the method has grown in popularity and has found applications in many disciplines including granular materials, additive manufacturing, pharmaceuticals, polishing, and rock mechanics [15].

In DEM, the governing differential equations are the laws of motion governing translation and rotation of each particle coupled with the contact forces due to the adjacent particles in contact with it. There are two different types of contact methods - hard sphere and soft sphere. In the hard-sphere method, interacting particles are assumed to be rigid and no overlap is allowed. In the soft sphere method, overlap between the particles is allowed. For this study, EDEM™ software developed by DEM Solutions, Edinburgh, UK is used. In EDEM™, the soft sphere method is used to calculate the magnitudes of forces acting on the particles. This method is found to be more accurate than the hard-sphere method (see Buist et al. [16]).

Two of the most critical steps in DEM model development are the particle shape

selection and the selection of contact models that capture the interactions between particles. The elements in the model can have different forms and distribution over the working domain. The research by ZoltAn [17] states that, from a computational point of view, spherical 3D particles are the easiest to compute. Particles then can be perfectly rigid or elastic depending on the problem to be solved. The rigid and elastic (hard and soft) sphere interactions are illustrated in figure 2.1.

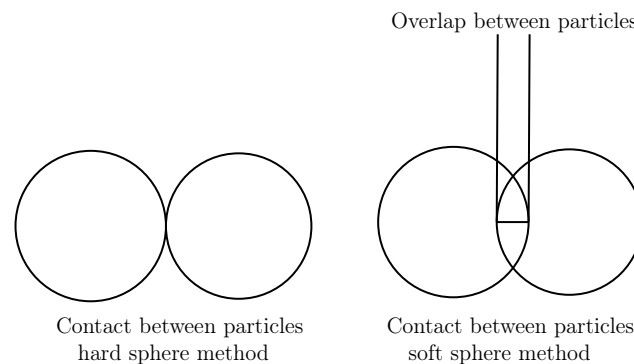


Figure 2.1: Hard and soft sphere contacts.

In DEM, there are different models depending on the properties of particle-particle and particle-geometry interactions. The generalized DEM model has the following major steps: particle generation, starting interactions (Moving Geometry and contact detection), contact force calculations and updating of the displacements and rotations of particles.

The choice of a specific contact model affects the contact and force. The model defines how the contact is detected and what parameters are used to execute the DEM algorithm. DEM algorithm is a sequence of calculations. A geometry is added and contact model and boundary conditions are specified. After initial step, the material properties, such as particle size, density, coefficient of restitution, coefficient of friction are defined. The next step is to identify the particles in contact which gives the contact forces generated between the particles. The user needs to define the kinematics of the geometry which in the present case is the speed of the blade to spread the powder. The algorithm then calculates the body and the external forces which are acting on

the particles. The last step in the algorithm is to calculate the accelerations and the velocities of the particles. Based on the velocities, the displacement vector of each particle is updated. The algorithm is repeated until the specified simulation time is reached. The flow-chart shown in figure 2.2 summarizes this process.

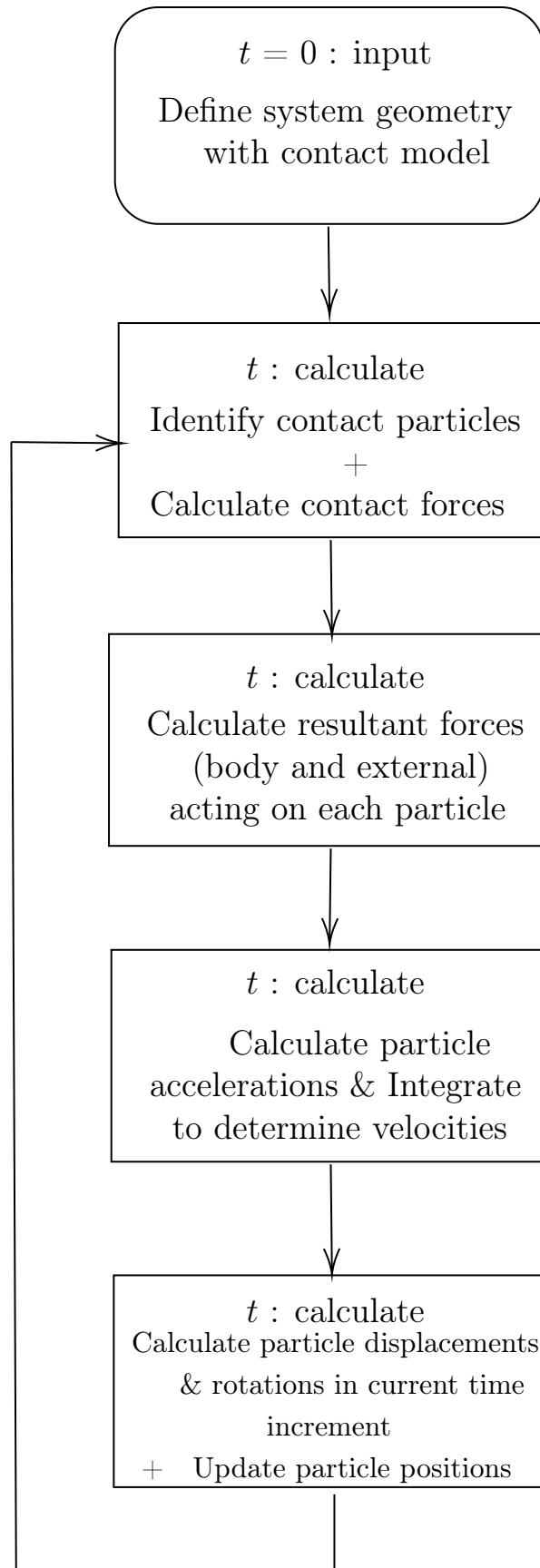


Figure 2.2: The general algorithm used in DEM calculations. [18]

## CHAPTER 3: DEM IN EDEM

In this work, DEM is applied to the powder spreading process to study the behaviour of the powder as it is spread over the powder-bed. The powder behavior is a cumulative effect of the interactions between particles and the particle-equipment interactions. This is done using contact models. In EDEM™, a soft sphere approach is used to model particle contact (see figure 2.1). The contact models used in this work are explained in detail in section 3.1.

### 3.1 DEM Simulation in EDEM

In EDEM™ simulation, different libraries are called for performing the calculations. The libraries or specific user-defined libraries connect different stages depending on where the library belongs. If needed, this process is carried out before running the primary function. The figure 3.1 gives an idea of how the simulation is carried out in EDEM™ and when an appropriate library is plugged in for calculations.

As seen from the figure 3.1 there are following main stages in the simulation performed in EDEM

1. The simulation initiates by the creation of geometry either in EDEM™ or is imported in standard CAD format
2. After the geometry creation, the user creates a custom factory. A factory is a place from where the particles are generated. It is a virtual geometry. For this EDEM™ imports particle generation library. There are two types of factories - dynamic and static. In dynamic factory as seen in figure 3.2, the particles are generated at a specified rate and keep on generating until the specified number of particles or mass is generated. In the static factory, the user defines a virtual

geometry where only the number of particles are generated which fits into the factory. As shown in figure 3.3 the particles occupy the space provided for generation and settle down if the boundary condition of gravity is specified.

3. Contact detection and contact calculation are performed after the particles are generated. Contact detection is particle-particle as well as particle-geometry contacts. At a given time a particle may have more than one contact. Contact calculation is performed by calling the contact model plugin for each contact.
4. Forces are calculated by calling the force plugin after the contacts have been calculated. Here, particle body forces are executed first irrespective of their presence in the user-defined library or the plugin.
5. After calculating the contacts and forces the particle positions need to be updated for the current time step.
6. The entire process is repeated until the given time is completed or until the availability of time steps.

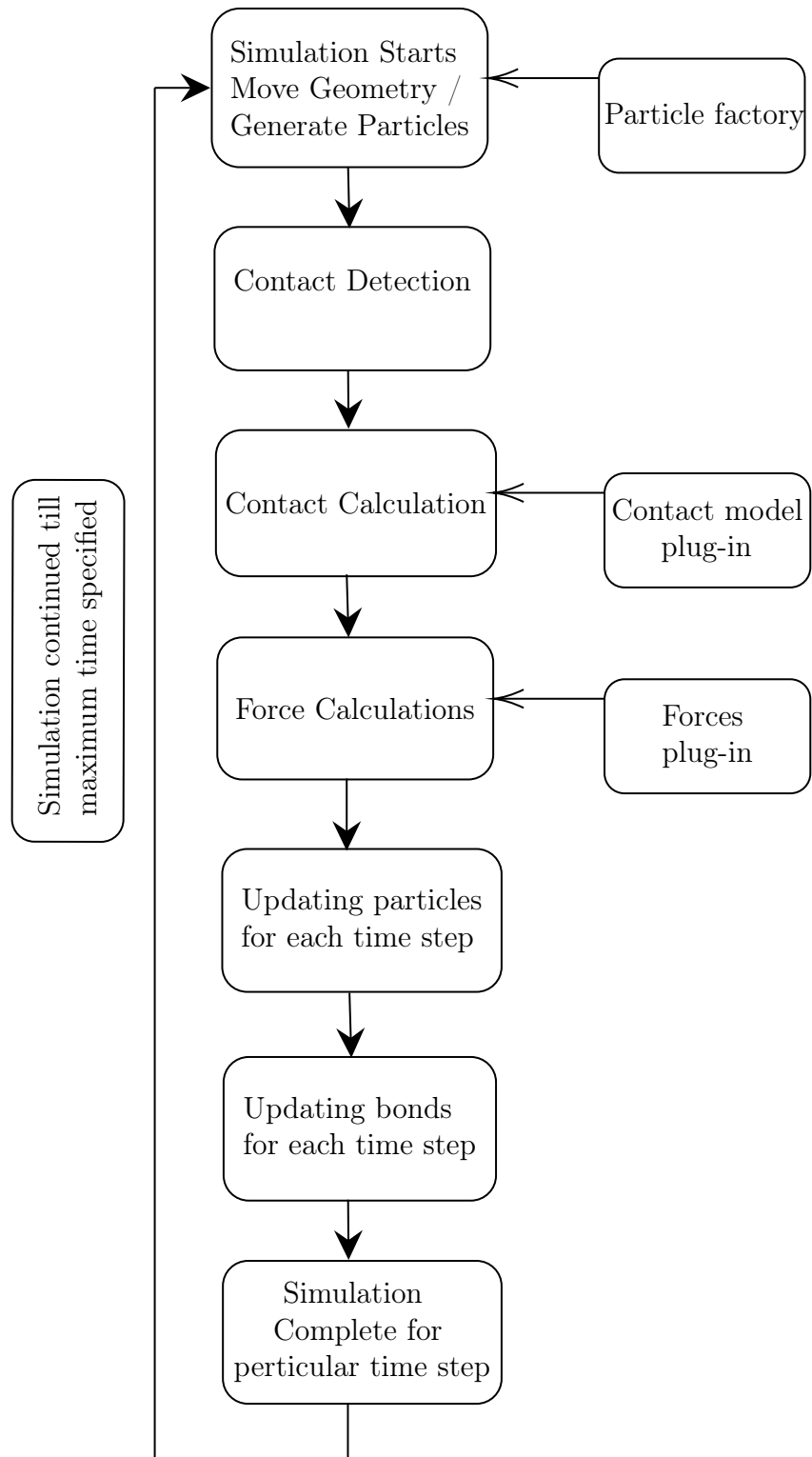


Figure 3.1: Simulation / Calculation Sequence in EDEM™ [1].



Figure 3.2: Dynamic Factory in EDEM.

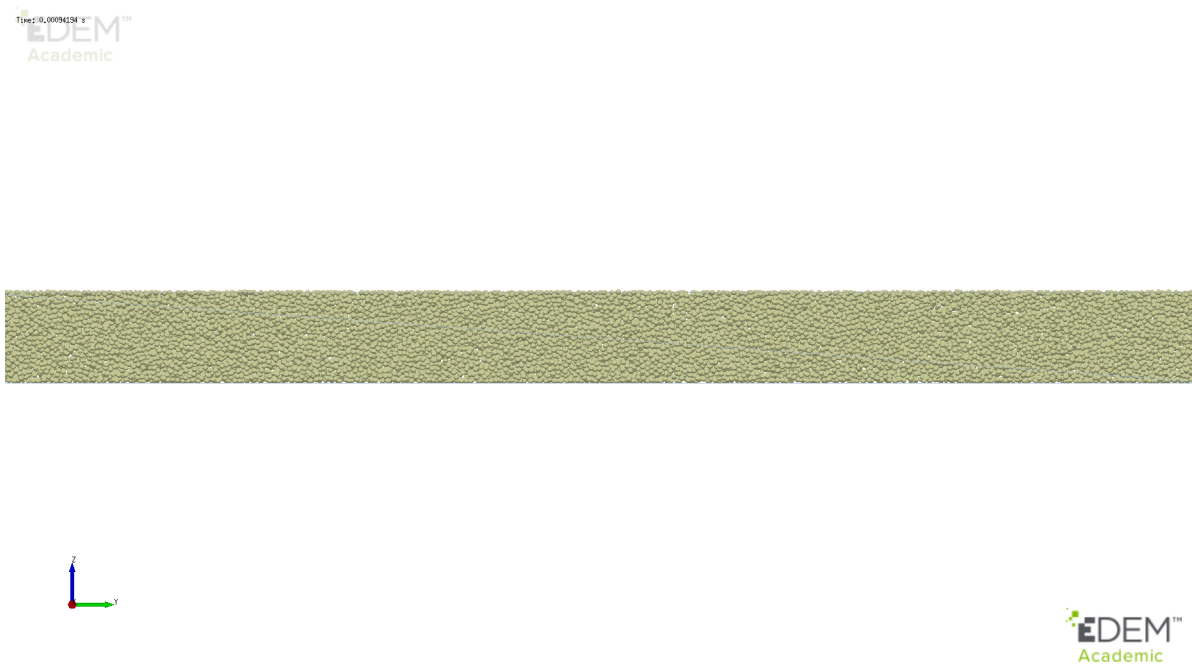
### 3.2 Contact Models

In DEM, a large number of particles considered are in contact or may come in contact. To study the behaviour of the powder, the contact and the particles forces are calculated based on the contact. For this, the algorithm first determines the contact between the particles and calculates the contact forces. These series of calculations are called contact detection and contact resolution part of the analysis [18]. In this study, the following contact models are used:

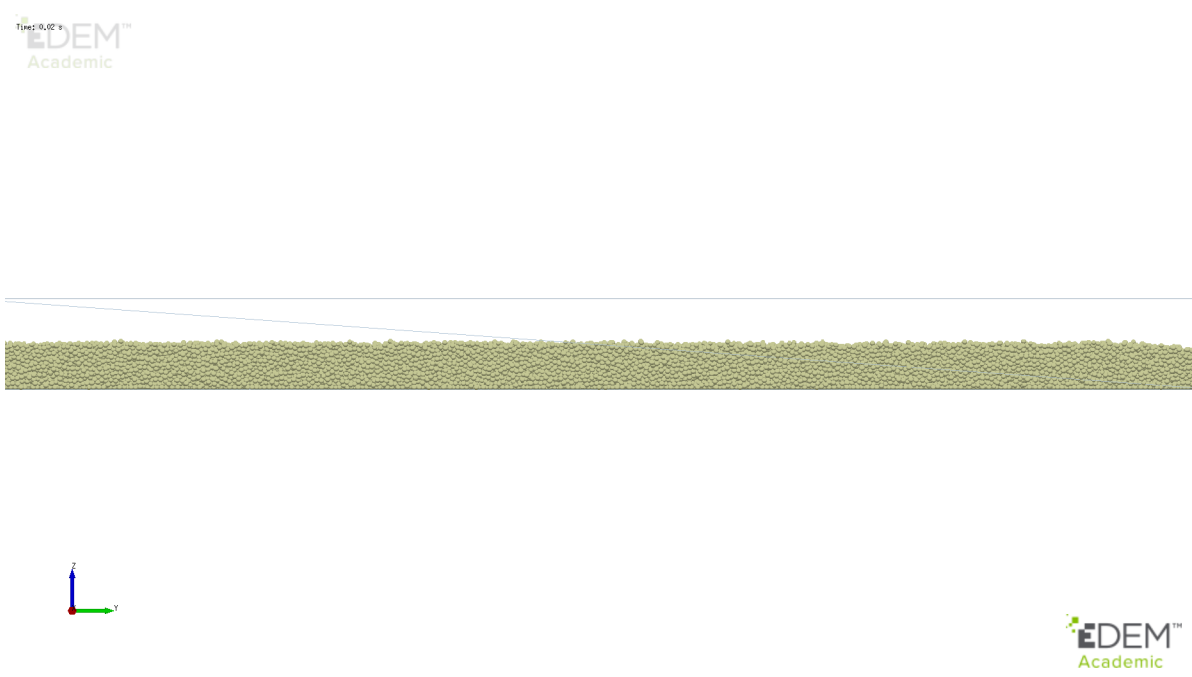
1. Hertz-Mindlin (no slip)
2. Hertz-Mindlin with JKR Cohesion.

The movement of the particles is calculated by the Newton's laws of motion. The equation given by Cundall and Strack [8] is: For Transnational motion,

$$m_i \frac{dv_i}{dt} = \sum F_{c,i} + m_i g, \quad (3.1)$$



(a) Static factory particle generation time step.



(b) Static factory after particle settled down.

Figure 3.3: Static Factory at two time steps.

Here,  $m$  is the mass of particle,  $v_i$  is the particle velocity,  $F_{c,i}$  the contact forces and  $g$  being the acceleration due to gravity. And for rotational motion,

$$\frac{d(I_i \cdot \omega_i)}{dt} = R_i \sum M_{c,i}. \quad (3.2)$$

Here,  $I$  is the moment of inertial of particle with respect to another,  $\omega$  is the angular velocity,  $R$  is the radius between the particles,  $M$  is moments acting on the particles.

### 3.2.1 Hertz-Mindlin contact model in EDEM

Hertz-Mindlin model is used to describe the particles in absence of cohesion. For calculating the tangential and normal direction forces, this model assumes spring-dash-pot system between two particles to consider all three-dimensional interactions. This model is a combination of Hertz contact theory and Mindlin-Deresiewicz theory. The normal forces are given by the Hertzian contact and the Mindlin and Deresiewicz theory gives us the tangential forces. In this model, the rolling friction is implemented and the normal and tangential components of forces are related to the coefficient of restitution via damping components [19]. Figure 3.4 represents the Hertz-Mindlin contact model.

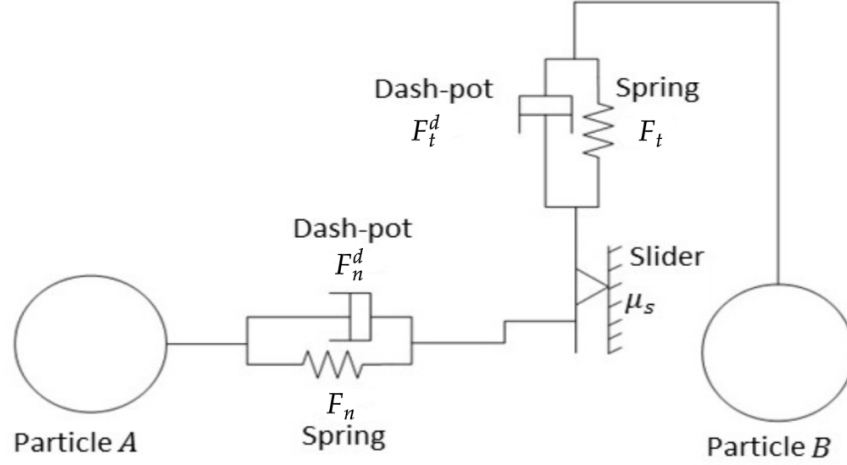


Figure 3.4: Hertz-Mindlin Contact Model [2].

Here, the normal force is given by  $F_{nor}$  and the tangential force is given by  $F_{tan}$ . These forces are calculated as the sum of their respective spring forces  $F_n$  or  $F_t$  and damping forces  $F_t^d$  or  $F_n^d$  such that:

$$F_{nor} = F_n + F_n^d \quad (3.3)$$

and

$$F_{tan} = F_t + F_t^d. \quad (3.4)$$

The normal force due to spring is given by,

$$F_n = \frac{4}{3} E^* \sqrt{R^* \delta_n^{\frac{3}{2}}}. \quad (3.5)$$

Where,  $E^*$  &  $R^*$  are given by,

$$\frac{1}{E^*} = \frac{1 - \nu_i^2}{E_i} + \frac{1 - \nu_j^2}{E_j} \quad (3.6)$$

and

$$\frac{1}{R^*} = \frac{1}{R_i} + \frac{1}{R_j}. \quad (3.7)$$

Here,  $E_i, E_j, \nu_i, \nu_j, R_i, R_j$  are Young's modulus, Poisson ratio, Radius of each sphere in contact respectively.

Tangential damping is given by,

$$F_n^d = -2\sqrt{\frac{5}{6}}\beta\sqrt{S_t m^* v_t^{rel}}. \quad (3.8)$$

Here,  $E^*$  is the equivalent Young's Modulus of the two particles into consideration.  $R^*$  is the equivalent radius, normal and tangential overlap are given by  $\delta_n$  and  $\delta_t$  respectively.  $\beta$  is the damping ratio which is related to the coefficient of restitution.  $m^*$  is the equivalent mass.  $v_n^{rel}$  and  $v_t^{rel}$  are the normal and tangential components of relative velocity respectively. The tangential force  $F_t$  depends on the tangential overlap  $\delta_t$  and tangential stiffness  $S_t$  as follows:

$$F_t = -S_t \delta_t. \quad (3.9)$$

The tangential damping force  $F_t^d$  is given by,

$$F_t^d = -2\sqrt{\frac{5}{6}}\beta\sqrt{S_n m^* v_n^{rel}}. \quad (3.10)$$

Here,  $\beta$  and  $S_n$  are given by a specific relation according to the Hertz-Mindlin theory and  $m^*$  is equivalent mass given by,

$$m^* = \left( \frac{1}{m_a} + \frac{1}{m_b} \right)^{-1}, \quad (3.11)$$

$\beta$  is given by,

$$\beta = \frac{\ln e}{\sqrt{\ln^2 e + \pi^2}}, \quad (3.12)$$

with  $e$  being the coefficient of restitution. The normal stiffness  $S_n$  and tangential stiffness  $S_t$  are given by,

$$S_n = 2E^* \sqrt{R^* \delta_n} \quad (3.13)$$

and

$$S_t = 8G^* \sqrt{R^* \delta_t}. \quad (3.14)$$

Here,  $G^*$  is equivalent shear modulus and is given by the following formula in which  $G_i$  and  $G_j$  are shear modulus of particles in contact given by,

$$\frac{1}{G^*} = \frac{2 - \nu_i}{G_i} + \frac{2 - \nu_j}{G_j}. \quad (3.15)$$

### 3.2.2 Hertz-Mindlin with JKR Cohesion

Cohesion is a property resulting in the attraction between particles of the same material. It was observed that the Hertz model by Derjaguin was inefficient to calculate the contact forces in the presence of cohesive energy between particles, but it provided a ground for further research. This model was not able to calculate the cohesive forces for the particles other than rigid ones. On the other hand, the JKR model in addition to Hertz-Mindlin, takes particle deformation into consideration with contact stress as well as cohesion. To include cohesion forces between particles in DEM simulations, JKR model is best suited [20].

Cohesion in powder flow plays an important role in determining the ease of flow, the post flow quality of powdered bed and the angle of repose. Cohesion between the particles increases with a decrease in the particle size [21]. As the particles tend to stick together during the flow, there is a need to calculate the parameters such as contact, contact forces, acceleration, velocity and displacement of the particles while solving the DEM algorithm.

This model considers the effect of Van der Waals forces which are present in the area

of contact between the particles. As this model accounts for cohesion between the particles, the normal elastic force is from JKR theory. As seen in Hertz-Mindlin (No Slip) model above, this model also follows the same steps of calculating forces [19].

1. Tangential elastic force
2. Normal dissipation force
3. Tangential dissipation force.

In JKR theory, the force depends on two parameters namely, overlap  $\delta$  and surface energy  $\gamma$ . The relation between these two parameters is given by,

$$F_{JKR} = -4\sqrt{\pi\gamma E^*}a^{\frac{3}{2}} + \frac{4E^*}{3R^*}a^3, \quad (3.16)$$

$$\delta = \frac{a^2}{R^*} - \sqrt{\frac{4\pi a}{E^*}}. \quad (3.17)$$

Here,  $a$  is given by,

$$a = \left( \frac{3F_n R^*}{4E^*} \right). \quad (3.18)$$

As observed in the above equation, Hertz-Mindlin force is obtained when the value of surface energy  $\gamma$  equals 0. Cohesion between particles exists even if they are not physically in contact. This model takes into consideration the gap between the particles for cohesion to exist. When the gap between the particles is more than the critical gap,  $\delta_c$  the cohesive force will be 0. It is given by,

$$\delta_c = -\sqrt{\frac{4\pi a_c}{E^*}} + \frac{a_c^2}{R^*}, \quad (3.19)$$

Here  $a_c$  is given by,

$$a_c = \left[ \frac{9\pi\gamma R^{*2}}{2E^*} \left( \frac{3}{4} - \frac{1}{\sqrt{2}} \right) \right]^{\frac{1}{3}}. \quad (3.20)$$

The maximum force when particles are separated by the gap less than the critical gap is called the pullout force which is given by,

$$F_{pullout} = -\frac{3}{2}\pi\gamma R^*. \quad (3.21)$$

## CHAPTER 4: SIMULATION SETUP IN EDEM

The simulation setup for the DEM study has two main components, the bed on which the powder is spread and the blade which spreads the powder. The bed and the blade size for modelling is scaled to make the simulation faster. Length of the bed is divided into two parts namely accumulation and spreading. The setup looks as shown in the figure 4.1.

The scale for the figures where the computational models are described is proportional to the particle size. Blade size is  $90D$ , bed size is  $600D$  in length and  $10D$  in width.

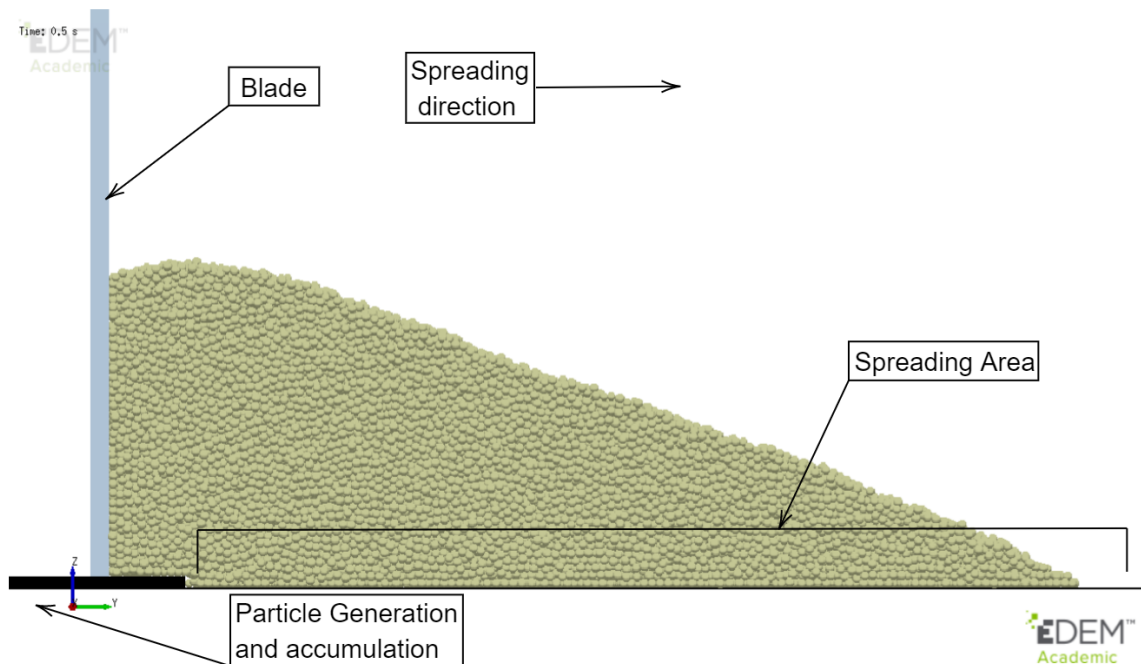


Figure 4.1: Simulation Setup.

## 4.1 Material Properties

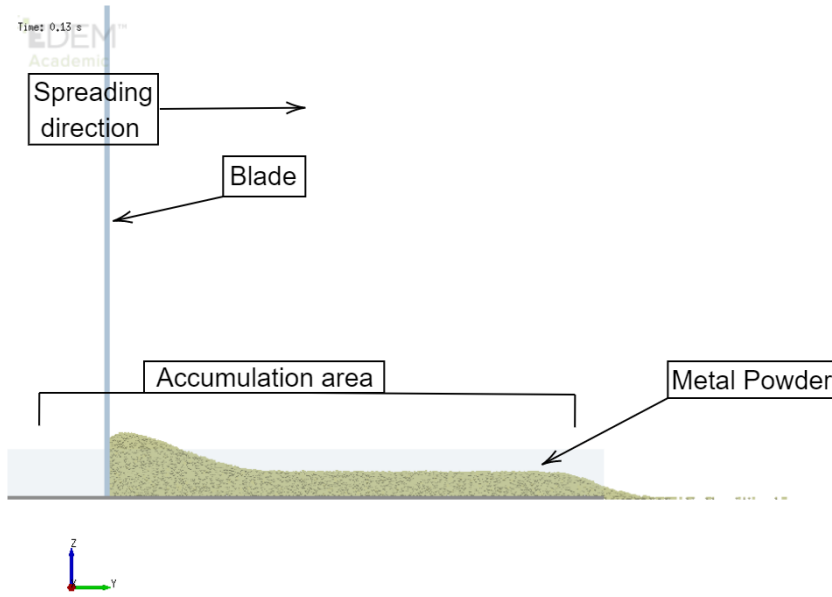
The material for the powder and the geometry used is stainless steel with the properties shown in table 4.1. Actual value of Young's modulus is 211 GPA which is measured by Ghadiri for bulk material [22]. Considering this large value makes the time step in DEM simulation very small leading to unrealistically long simulation time as it makes the time step significantly small. To get achievable simulation time Young's modulus is brought down to 2.1 GPA. The calibration for reducing Young's modulus is experimentally performed by Behjani et al. [23], HÅŠrvg et al. [24] and Washino et al. [25] which is then summarized in [10].

Friction in this process is static and rolling friction. Static friction is responsible to hold the particles from translating and rolling friction is the one which resists rolling motion of the particles. The static friction coefficient is taken as 0.05 as measured in the experimental process performed by Nan et al. in [10]. In this study rolling friction is not studied for this it is taken as the lowest value possible which is 0.01. The coefficient of restitution which is not mentioned in the table below is one of the parameters studied in this work by considering 0.32 and 0.64 as the two COR values.

Table 4.1: Material Properties - Stainless Steel.

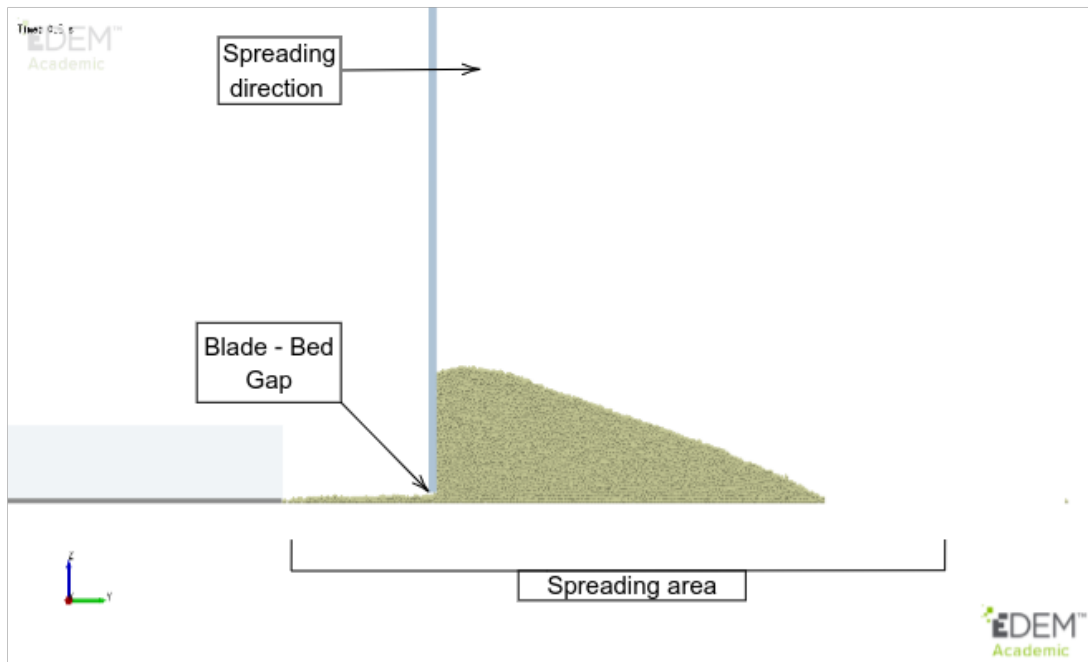
Property	Symbol/ Notation	Value
Poisson's Ratio	$\nu$	0.3
Young's Modulus	$E$	2.1e+09 Pa
Density	$\rho$	7980 Kg/m <sup>3</sup>
Coefficient of static friction	$\mu_s$	0.5
Coefficient of rolling friction	$\mu_r$	0.01

In the simulation of powder spreading the first part is to accumulate the particles forming a heap of the bulk material as seen in figure 4.2a. Next, the bed is constructed such that there is a step created which acts as the gap between the blade and the bed. This gap is varied for the parametric study in this work. As the blade continues to move forward the powder gets spread from the gap as shown in figure 4.2b.



EDEM™  
Academic

(a) Accumulation



EDEM™  
Academic

(b) Spreading

Figure 4.2: Simulation setup (Accumulation & Spreading).

## 4.2 Parametric Study

As discussed earlier, parametric study is performed to better understand the process and to obtain the relation between these parameters and the packing density of powder on the bed. The parameters studied for this process are as mentioned in table 4.2. Typically the COR value of powder is 0.64 to examine how it affects the process 0.32 was considered as well. Similarly for surface energy values are varied by 20% from typical value of 1.4 (mJ/m<sup>2</sup>).

Table 4.2: Material and Process Parameters.

Blade Speed (m/s)	Gap - Blade - Bed ( $\delta/D$ )	COR (e)	Surface energy $\gamma$ (mJ/m <sup>2</sup> )	Particle Size Distribution (Normal) ( $\mu\text{m}$ ) <sup>1</sup>	Particle diameter $D$ ( $\mu\text{m}$ )
0.05	1.5	0.32	0	None	50
0.08	2.5	0.64	1.2	M - 90 SD - 18	90
0.1	3		1.4	M - 90 SD - 18 (with cap <sup>2</sup> )	120
0.12	4		1.6	M - 120 SD - 24	
0.16				M - 50 SD - 10	

Here,  $\delta$  is the gap between blade and bed,  $D$  is the particle diameter,  $\gamma$  is the surface energy of the material, COR is the coefficient of restitution.

<sup>1</sup>M stands for mean, SD stands for standard deviation

<sup>2</sup>Distribution capped with mean as 90  $\mu\text{m}$  lower limit as 60 $\mu\text{m}$  and upper limit as 120 $\mu\text{m}$

## CHAPTER 5: RESULTS AND DISCUSSION

This chapter aims to study the powder spreading behaviour concerning the parameters which were varied. The quantities observed will be packing density and mass flow rate through the blade - bed gap. The parameters varied are as shown in table 4.2.

### 5.1 Mass flow rate (MFR)

The mass flow rate of the powder gives an idea of how good the particle flow is during spreading. As the mass flow increases the packing density increases giving a better powdered bed meaning less voids. Mass flow rate is studied by varying the blade speed, blade - bed gap, COR and the surface energy of the powder. Theoretically the mass flow rate of the powder is given by the following formula:

$$MFR = \rho VA. \quad (5.1)$$

where  $\rho$  is the material density of the powder,  $V$  is velocity and  $A$  is the area which it is flowing through.

In this study, the mass flow rate is being calculated by an inbuilt sensor in EDEM™ software. It is aligned such that it covers the particles flowing exactly below the blade. The inbuilt sensor considers each particle's velocity, mass and the size of the sensor to calculate the mass flow rate. The width of the sensor (bin) is same as the width of blade which is proportional to particle diameter. It is given as shown in equation 5.2.

$$\dot{M} = \frac{\sum(m_i(v_i \cdot \hat{l}))}{l}. \quad (5.2)$$

$\dot{M}$  = The magnitude of mass flow rate,  $m_i$  = The mass of particle  $i$  in the sensor (selected bin),  $v_i$  = The velocity of the particle  $i$  in the sensor (selected bin),  $\hat{l}$  = The length of the cylinder as a unit vector (length AB in fig 5.1).

For each particle, its mass is multiplied by the dot product of its velocity and the unit vector of the cylinder from start to end. These per particle values are then summed and divided by the length of the bin. The length of the bin is the distance from the start point to the endpoint of the cylinder.

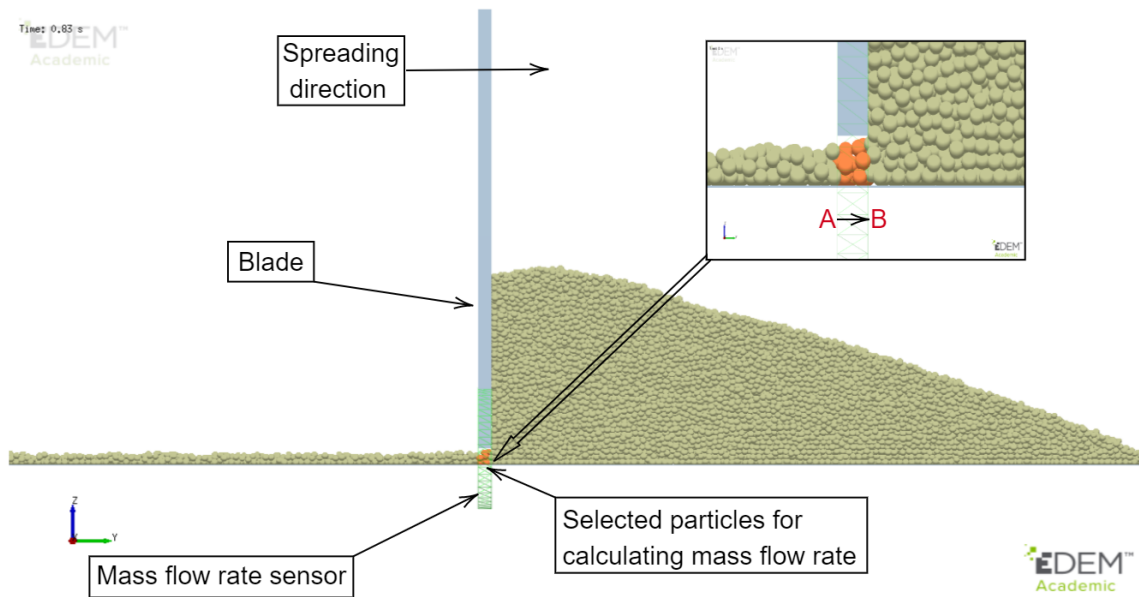


Figure 5.1: Mass flow rate (MFR) calculation setup.

## 5.1.1 Effect of mass flow rate on gap size for different speeds

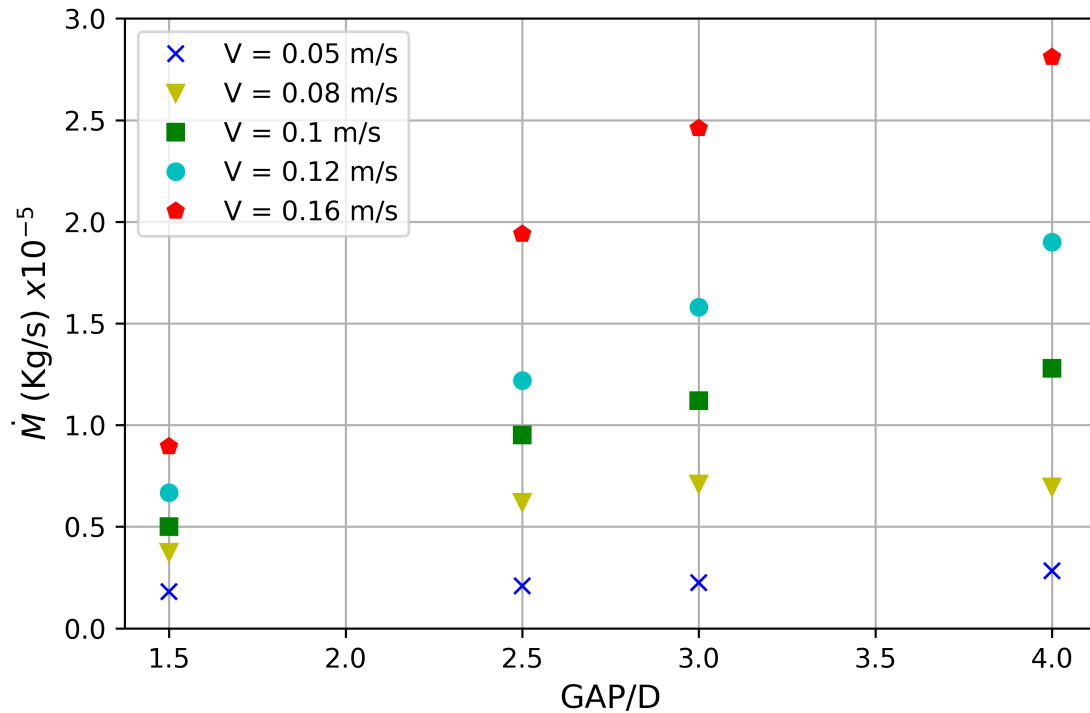


Figure 5.2: Mass flow rate (MFR) against Gap/ $D$  and different velocities.

The plot 5.2 shows the variation of mass flow rate concerning different blade - bed gap for different blade speeds. For this study the parameters were set as COR of 0.64, surface energy of 1.4 mJ/m<sup>2</sup>, normal particle size distribution with mean as 90  $\mu\text{m}$  and standard deviation of 18  $\mu\text{m}$ . As observed from the plot, MFR increases with increase in velocity which is expected as it is directly proportional to the velocity. For blade - bed gap the mass flow rate increases with increase in the gap size. This is because as the gap gets larger more particles tend to fit in it and flowing away from the bed. It should be noted that even though the mass flow rate for higher speeds is more it won't help increase packing density. This will be discussed in section 5.2.1.

## 5.1.2 Study of COR on mass flow rate

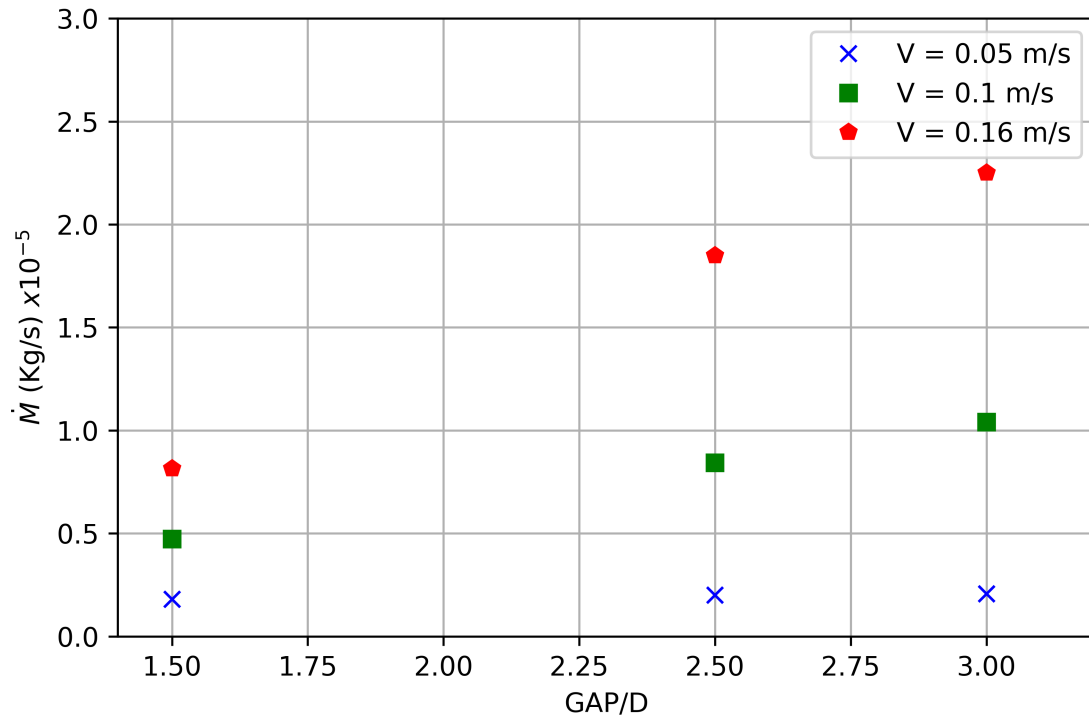


Figure 5.3: Mass flow rate (MFR) against Gap/ $D$  and different velocities and COR.

One of the parameters varied for the parametric study is coefficient of restitution COR ( $e$ ). COR is the ratio of relative velocity after and before collision between the particles. It is a material property and ranges from 0 to 1. If the value of ( $e$ ) is 0 it is perfectly inelastic collision and perfectly elastic for  $e$  equals 1. The plot in fig 5.3 shows relation between COR affects and the mass flow rate. Mass flow rate is not majorly affected with change in COR which was decreased from 0.64 to 0.32. The rest of the parameters are same as section 5.1.1. Also, it can be inferred that as COR does not affect MFR the trend will be similar for gap size of  $4D$  and blade speed of 0.08 and 0.12 m/s.

## 5.1.3 Study of particle size on mass flow rate

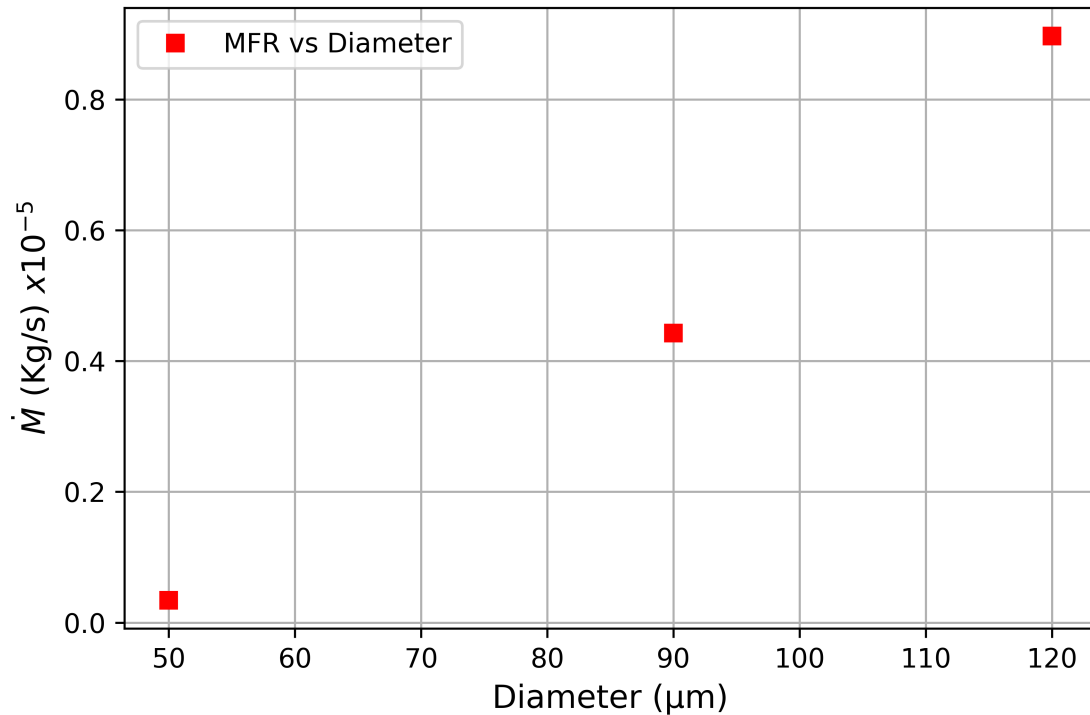


Figure 5.4: Mass flow rate (MFR) against particle diameter  $D$ .

To study the effect of particle diameter on mass flow rate parameters from 5.1.1 and COR of 0.64 was used with three different particle diameters of 50, 90 and 120  $\mu\text{m}$ . As the particle diameter decreases the effect of cohesion is more, which can also be seen from equation 3.16. Increase in the cohesive forces decreases the fluidity of the particles. Thereby making it difficult to pass through the gap as they tend to stick to each other leading to decrease in mass flow rate. This can be observed in the plot 5.4 where the mass flow rate is highest for particle size (diameter) of 120  $\mu\text{m}$  followed by 90 and 50  $\mu\text{m}$  size particles. This trend is examined by taking the packing density average values after the spreading was complete.

## 5.1.4 Effect of surface energy on mass flow rate

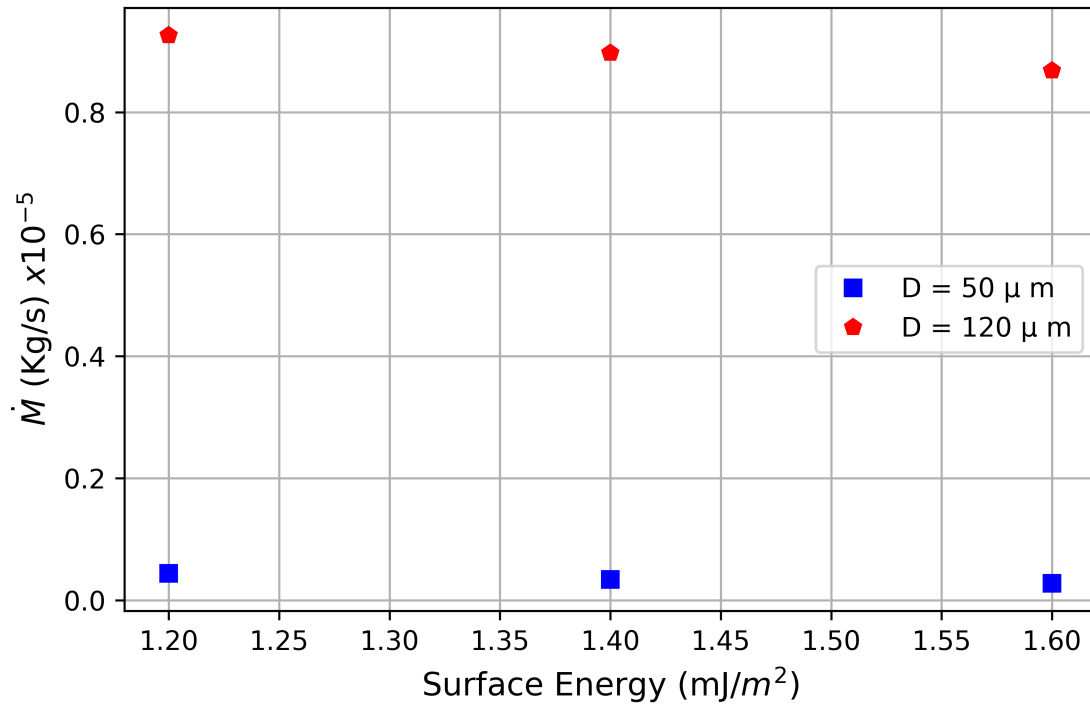


Figure 5.5: Mass flow rate (MFR) against surface energy.

Surface energy can be defined as the work required to cut or separate a bulk sample. From equation 3.16 in Hertz-Mindlin with JKR contact model it is seen that as surface energy increases the cohesive force between the particles increases. Making it difficult for them to separate. For studying how mass flow rate is affected by change in surface energy, it was varied by about 20% from 1.4 mJ/m<sup>2</sup>. Simulations were carried out with values of parameters from 5.1.1, COR of 0.64 and with surface energy varying as 1.2, 1.4 and 1.6 mJ/m<sup>2</sup>. As discussed earlier in figure 5.1.3, surface energy has higher impact on smaller sized particles. Therefore, for this study particle sizes of 50 and 120 μm were used. As observed, the mass flow rate tends to decrease with increase in surface energy and affects more for 50 μm particle size.

## 5.2 Packing Density

Packing density of the particles determines how well the final product will turn out in terms of surface finish and less cavities [12]. For this study, packing density is measured after the spreading process as shown in figure 5.6. Packing density is given by,

$$\text{Packing density (PD)\%} = \frac{\text{Total volume occupied in bin by particles}}{\text{Total volume of the bin}} \times 100. \quad (5.3)$$

The setup to measure the packing density is shown in figure 5.6. A box bin is set up on the bed, which gives value of volume occupied by the particles on the bed. It is then divided by volume of bin and multiplied by 100 as shown in equation 5.3. The maximum theoretical value of packing density found was between 50% to 70% in the study by [6]. One of the way of measuring theoretical packing density for particles with different size is by packing them in a cube with known volume.

The box bin was set up in such a way that it does not consider the particles which are near the blade as they have not yet settled and may move forward as they have a velocity in the direction of the blade. This setup is shown in fig 5.6.

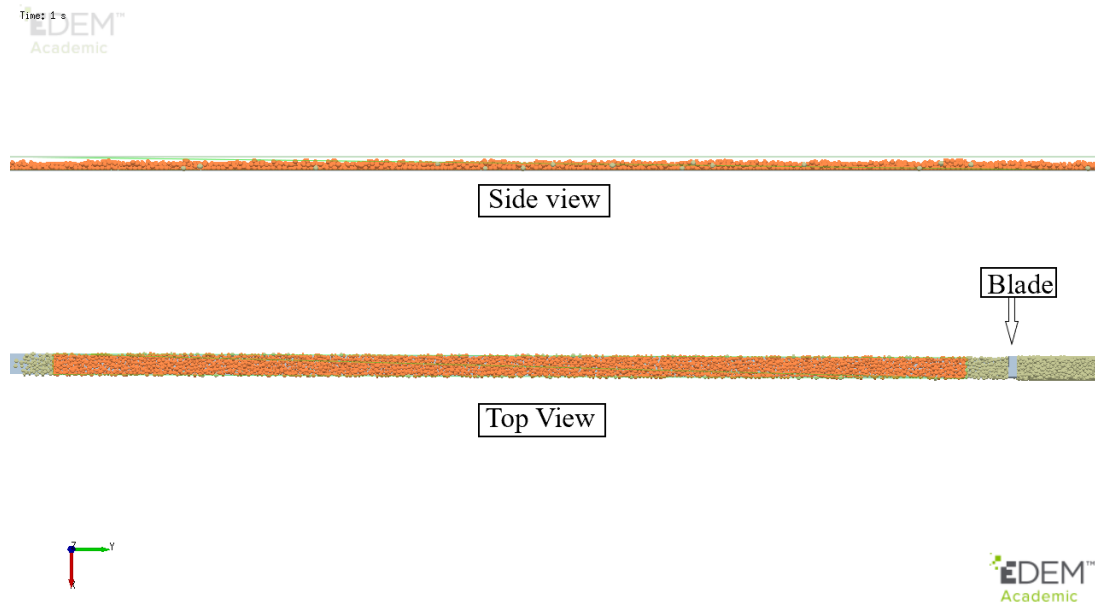


Figure 5.6: Packing density (PD) setup.

### 5.2.1 Effect of gap on PD for different gap sizes and velocities

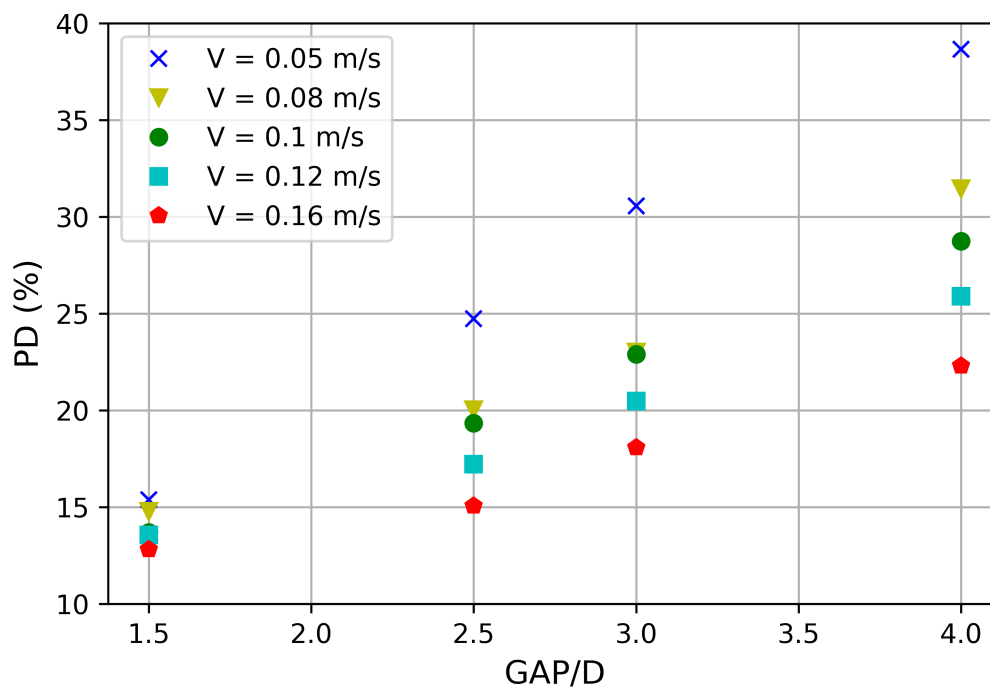


Figure 5.7: Packing density (PD) against Gap/ $D$  and different velocities.

Plot 5.7 shows the effect of different gap sizes on the packing density for different speeds. It was observed that as the gap increases the packing density increases. It was expected because as the gap gets bigger there is more space available to flow through it. Also, as the blade speed increases, the packing density decreases. This phenomenon occurs as the particles have higher speed and there is less time to flow through the gap. The particles spreaded have higher velocities in the direction of the blade, due to which they do not settle quickly and continue travelling in the same direction resulting in less packing density. For this study other parameters were set as COR - 0.64, surface energy - 1.4 mJ/m<sup>2</sup>. And normal particle size distribution, with mean as 90  $\mu\text{m}$ , particle diameter as 90 $\mu\text{m}$  along with standard deviation of 18  $\mu\text{m}$ .

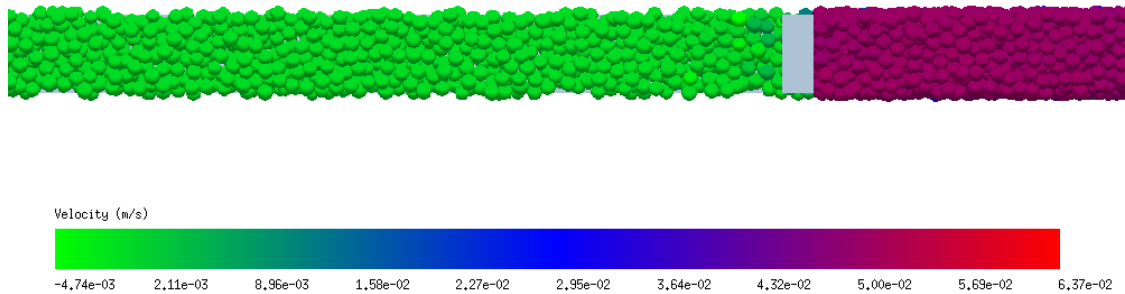


Figure 5.8: Particle velocities after spreading for blade speed 0.05 m/s.

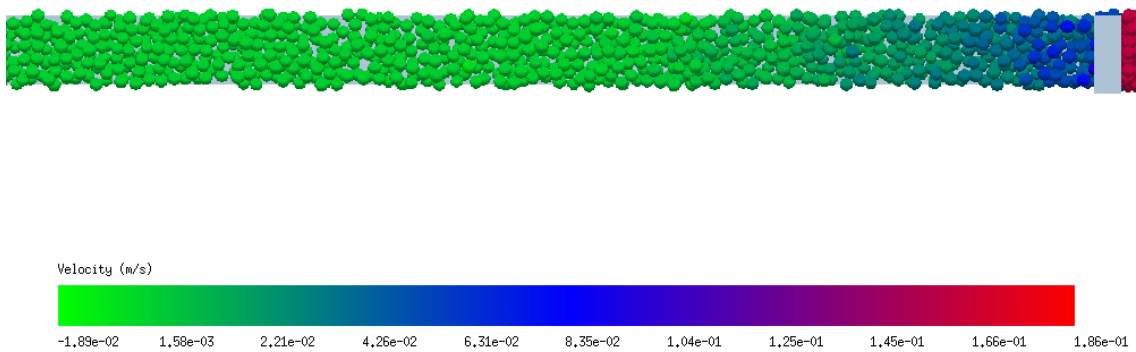


Figure 5.9: Particle velocities after spreading for blade speed 0.16 m/s.

As discussed above, increase in the speed decreases the packing density due to particles having high speeds while spreading. From the figure 5.8 and figure 5.9 it is clear that as the blade speed is higher, particles tend to continue in the direction of spreading. Therefore, decreasing the packing density of the powdered bed. Periodic boundary conditions are used for sides of the bed so as the particle falls from one side of the bed it reappears exactly on the opposite side.

## 5.2.2 Packing density trend with change in COR

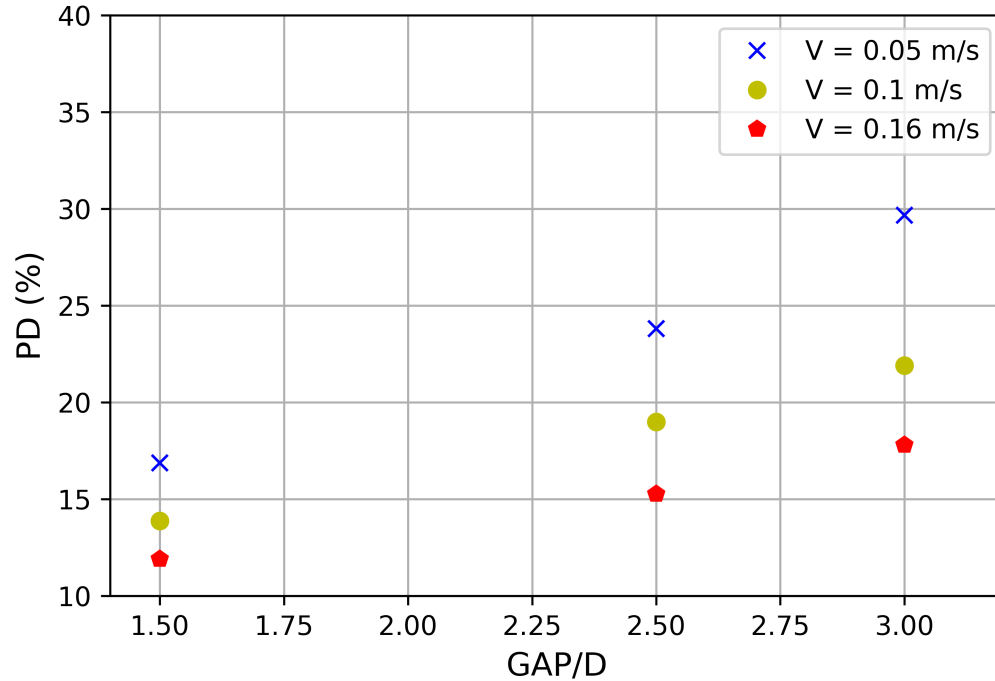


Figure 5.10: Packing density (PD) against Gap/ $D$  and different velocities and COR.

To observe the effect on packing density when the powder has different values of COR ( $e$ ), simulations were carried out and the same two values of COR 0.32 and 0.64 were considered. As seen in the plot 5.10 the packing density shows a similar trend of increasing with increase of gap and decrease of blade speed. Therefore from comparison of figure-plots 5.7 and 5.10, it can be inferred that packing density is not affected with change in COR. This tells that similar trend for gap of  $4D$  and blade speed of 0.08 and 0.12 m/s will occur for  $COR = 0.32$ .

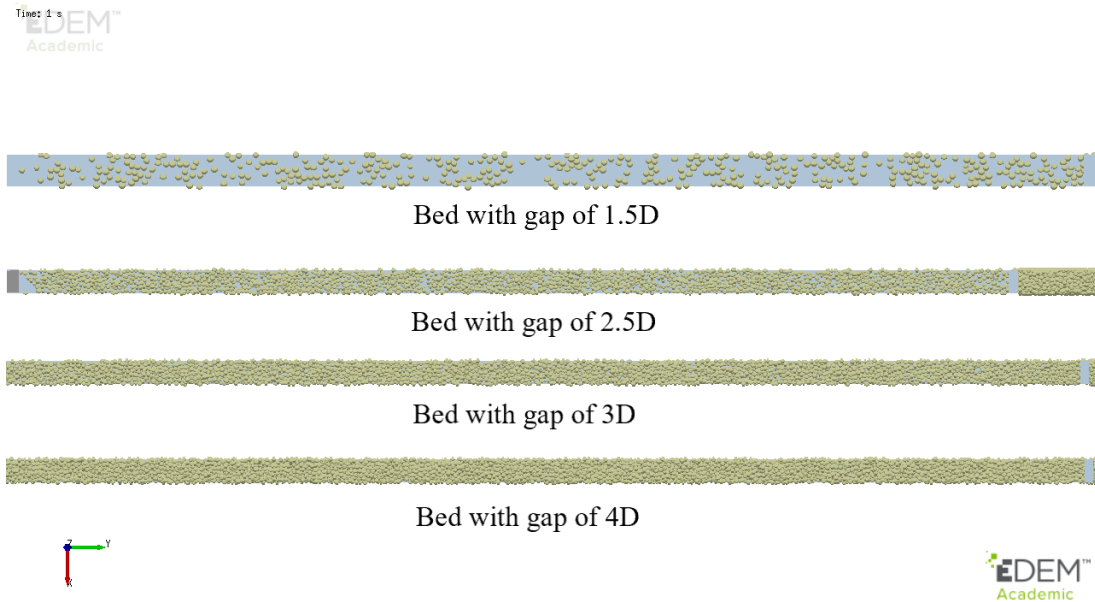


Figure 5.11: Powdered bed for different Gap size.

Figure 5.11 compares powdered bed for different gap sizes. Gap size of  $1.5D$  has maximum voids making packing density extremely low. For this comparison the blade speed is fixed to  $0.05 \text{ m/s}$  with rest of parameters as mentioned in section 5.2.1.

## 5.2.3 Change in packing density for different size particles

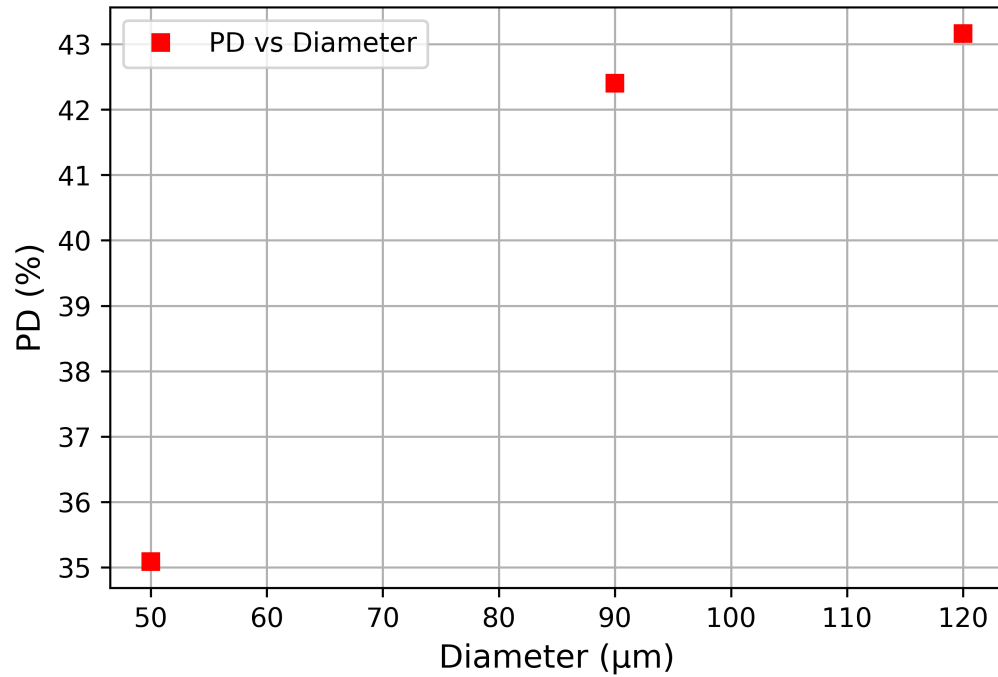


Figure 5.12: Packing density (PD) against particle diameter  $D$ .

It can be observed in above plots, that in the presence of surface energy the fluidity of smaller particles get restricted. To analyse the effect on packing density of particles, the input parameters are taken as mentioned in section 5.2.1 with COR as 0.64, gap of  $3D$ , blade speed as 0.05 m/s. From the plot 5.12, the packing density is less for smaller particle size because of cohesion effect being greater on them.

## 5.2.4 Surface energy and packing density

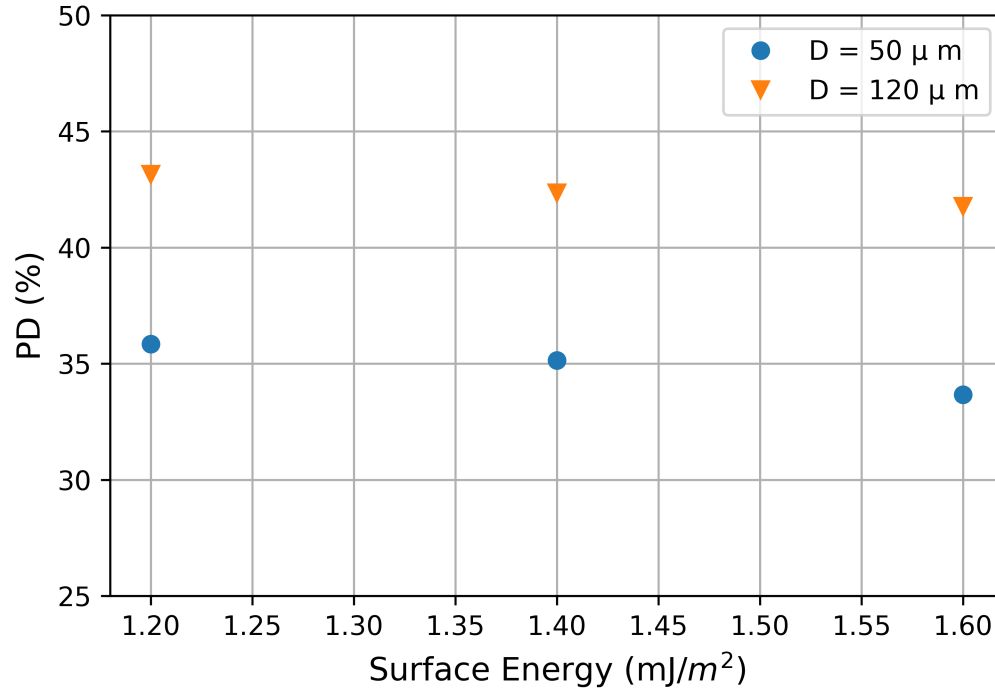


Figure 5.13: Packing density (PD) against surface energy.

To study how change in the surface energy impacts packing density, simulations were performed with parameters mentioned in section 5.2.3. With increase in surface energy, the cohesion force increases between particles which causes particles to stick together as in equation 3.16. Surface energy for this study has been changed by 20% from the value of  $1.4 \text{ mJ}/\text{m}^2$ , to check the change in trend of packing density. From plot 5.13, the packing density of powder after spreading decreases with increasing the surface energy, thus satisfying the mathematical relation.

### 5.2.5 Particle size distribution and Packing density

Particle size distribution plays an important role in packing density. If in a powder there are same size particles there will be voids between the particles, as there will be almost no percolation. Percolation is the phenomenon where smaller particles tend to fill the gaps between the larger sized particles during powder packing. Presence of smaller size particles in powder mixture increases the chances of percolation making positive impact on packing density. To study this phenomenon simulations with normal size distribution were carried out. In plot 5.14, the graph showing ‘Std Dev’ is for particles having normal distribution with mean  $90 \mu\text{m}$  and standard deviation of  $18 \mu\text{m}$ . For this, the particles size can range between negative infinity to positive infinity following the normal distribution bell curve. As studied in [6] percolation does not occur in presence of significantly larger particles with smaller ones. This leads to having low packing density as explained with wall effect phenomenon discussed in [12]. Larger size particles tend to form a structure such that other particles cannot penetrate into the gaps between these particles resulting in local voids, this phenomenon can be referred as wall effect. Generally the packing density of powder is around 50% which rarely goes up to 70% with optimized powder properties according to studies [26–28]. In order to increase the packing density, one way is to have specific size particles in the mixture. For this, one more simulation with same conditions as above but particle size distribution capped from both end of bell curve was carried out. In this smallest particle size of  $60 \mu\text{m}$  and largest particle size of  $120 \mu\text{m}$  was used as shown in the figure 5.15. From plot 5.14 of packing density vs dimensionless time, it can be inferred that by capping particle size distribution the packing density increases boosting the action of percolation. Here dimensionless or normalized time is necessary to compare two different simulations where the local spreading time is different. The local spreading time is given by  $(\text{bed length})/(\text{balde speed})$

Dimensionless time is calculated as -

$$\text{Dimensionless time} = \frac{\text{Difference between two local times}}{\text{Total spreading time}}. \quad (5.4)$$

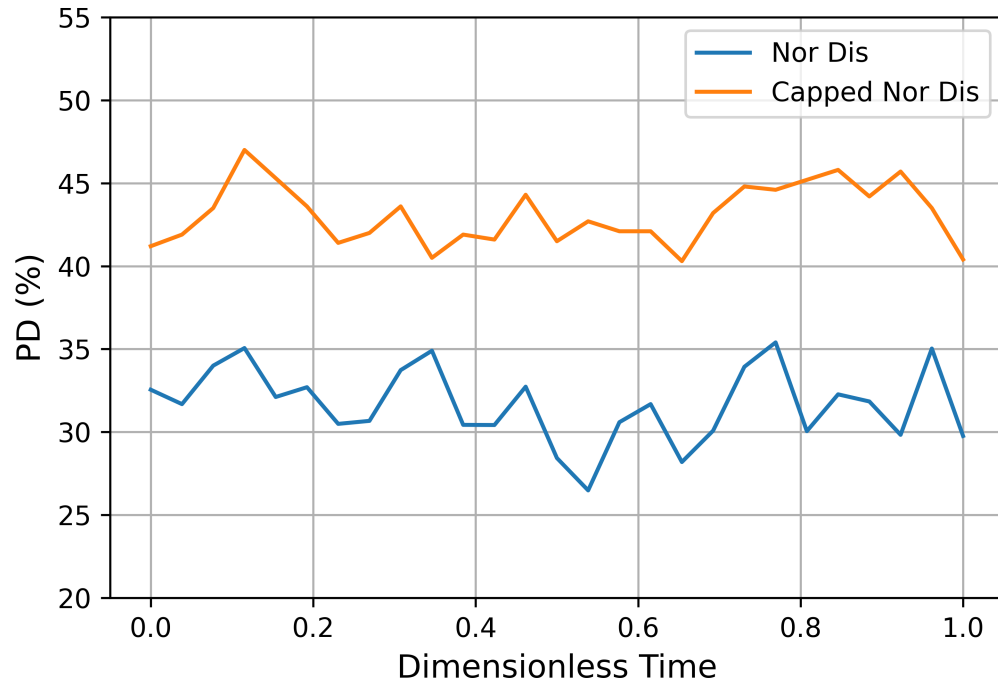


Figure 5.14: Packing density (PD) against capped and uncapped normal distribution.

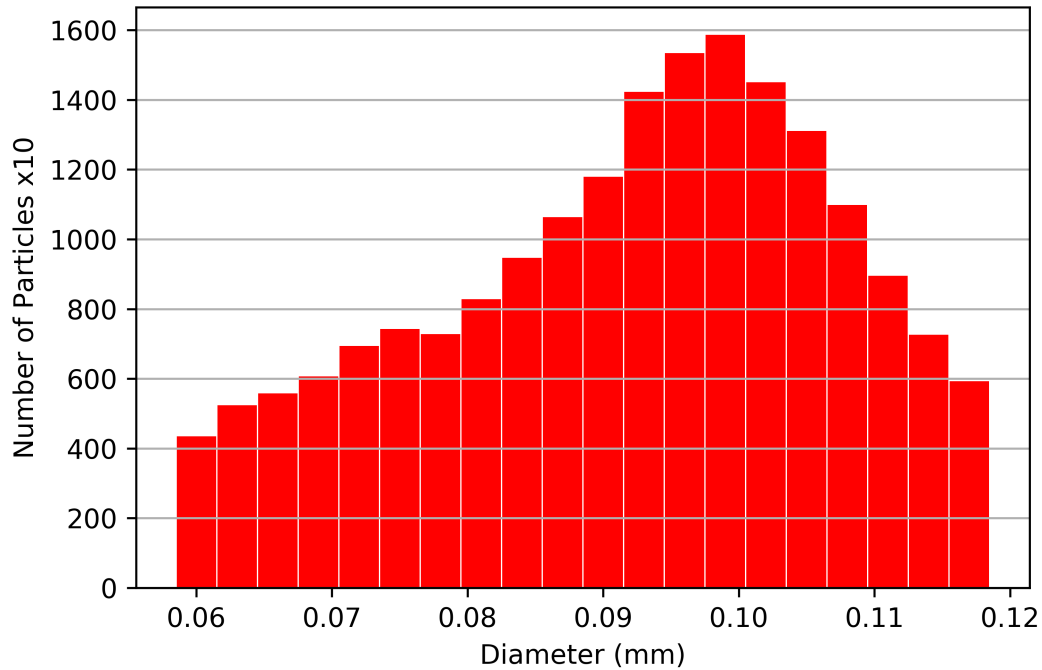


Figure 5.15: Capped normal distribution of particle diameter  $D$ .

### 5.3 Angle of repose study

Angle of repose of the powder gives an idea about the fluidity of the powder. The smaller the value, the better the fluidity of the powder [29] [30]. Angle of repose of a granular material can be defined as the slope made by the particles or material with respect to the horizontal plane or the angle which changes with the transition of the material [31] [32]. It is one of the crucial parameter to study material properties and has vast applications in geomechanics where, it has been particularly used to study the properties of sand.

In the figure 5.16 the setup to measure angle of repose at all time steps while spreading the powder is shown.

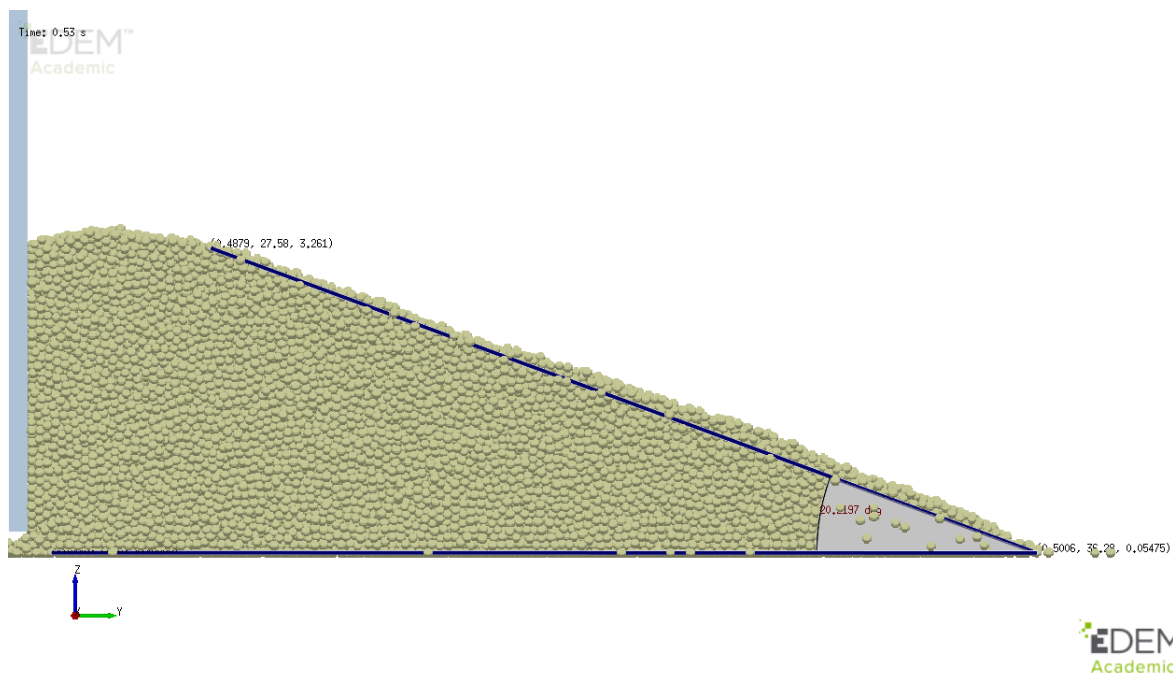


Figure 5.16: Angle of repose (AOR) setup.

### 5.3.1 Angle of repose and cohesion

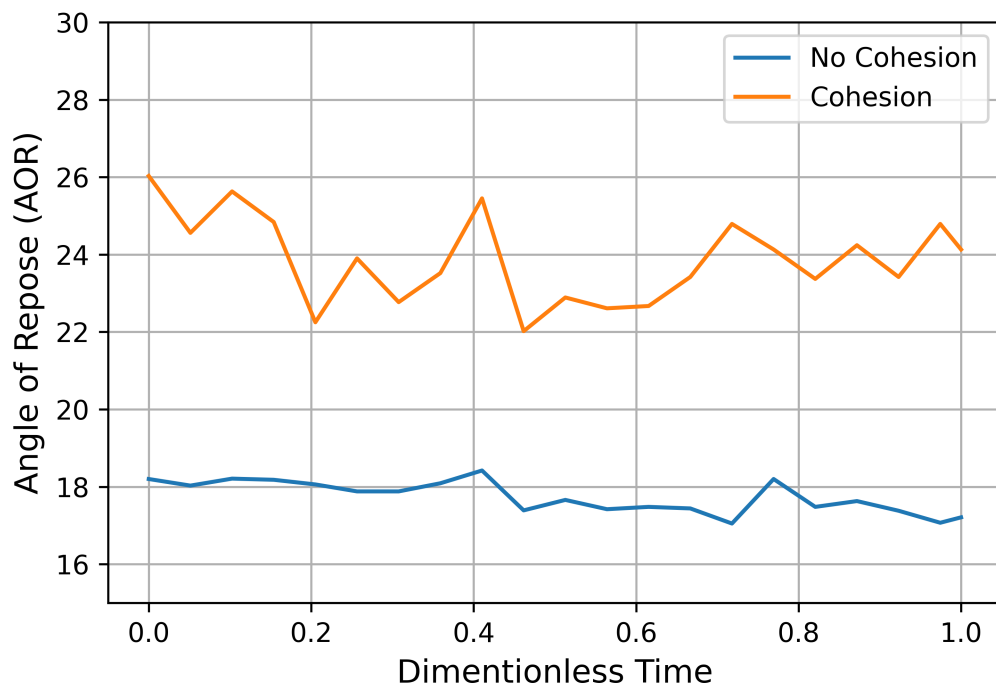


Figure 5.17: Angle of repose (AOR) with and without cohesion.

In the figure 5.17 angle of repose is plotted against dimensionless time. The graph of angle of repose with no cohesion, is the one with no surface energy. The one with cohesion is with JKR model or with presence of surface energy. From the figure it can be observed that angle of repose increases with cohesion, as particles tend to stick to each other giving a larger value of the angle.

### 5.3.2 Effect of gap and blade speed with angle of repose

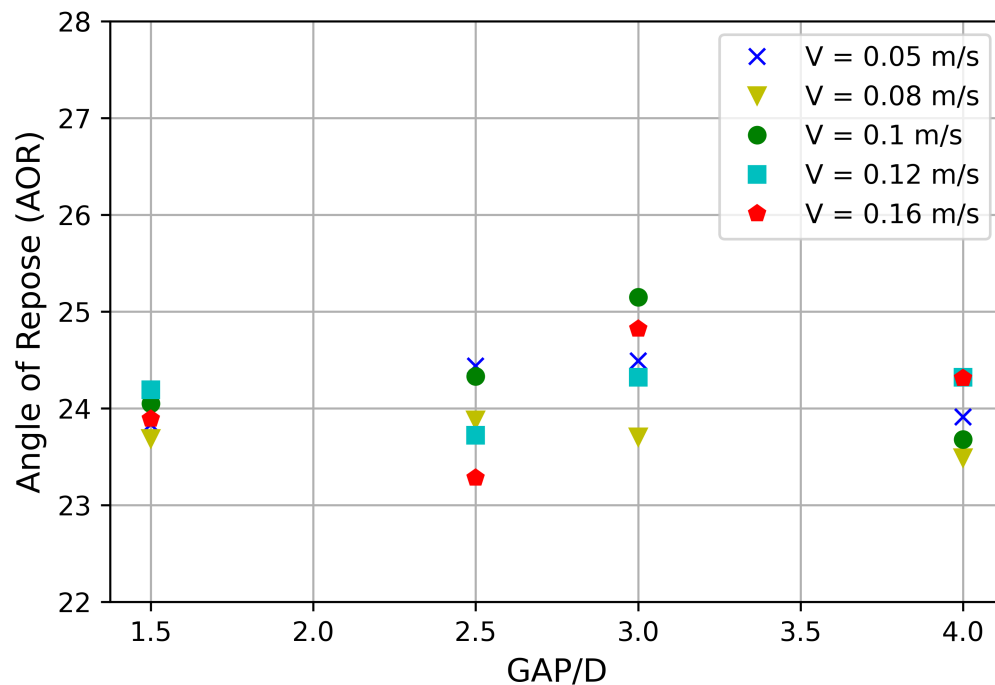


Figure 5.18: Angle of repose (AOR) against Gap/ $D$  and different velocities.

Angle of repose is a material property and does not depend on the process parameters. Figure 5.18 shows variation of angle of repose with respect to the blade - bed gap and blade speed. The values of angle of repose varies between  $23^\circ$  and  $25^\circ$  which proves that the angle of repose does not depend on the blade - bed gap and blade speed.

The study by Zhou et al in [33] shows that the angle of repose depends on factors

such as sliding friction and rolling friction of the material. It forms a larger connecting length making particles harder to slide over each other and forming a larger angle of repose.

## CHAPTER 6: CONCLUSIONS AND RECOMMENDATIONS FOR FUTURE WORK

### 6.1 Conclusions

This chapter summarizes the results obtained from this research. Powder spreading was successfully modeled in EDEM™ and simulations were carried out. Hertz-Mindlin and Hertz-Mindlin with JKR cohesion contact models were discussed along with the reason why they are used. EDEM™ was used because of its proven accuracy and ease of modelling using discrete element method.

Based on results presented in the previous chapter, the mass flow rate increases linearly until gap size of three times the diameter and tends to settle after that. Also, the mass flow rate increases with the blade speed for the particles directly below the spreader or blade. It was observed that change in the coefficient of restitution (COR) did not affect how the powder was spread and did not have any considerable effect on mass flow rate. Particle diameter plays an important role in this process. Generally small particles give good fluidity, but in the presence of cohesion it becomes difficult for them to separate from each other affecting the mass flow rate. In the same manner as the surface energy increases, the force of cohesion increases leading to the decrease in mass flow rate.

Packing density determines how well the powder is spreaded on the bed. This affect the manufactured part's quality making it one of the important factors for study. As discussed in the previous chapter, the packing density increases with increase in the gap. Therefore, it is recommended to not have blade - bed gap below three times the diameter, as it will have high number of void patches across the bed, which is not suitable for laser powder bed. Also, packing density decreases with the increase

in blade speed. This happens due to particles motion continuing with the same speed and taking time to settle after spreading process. Coefficient of restitution (COR) does not play any role in terms of packing density as well, giving similar trends and values when changed. As discussed earlier smaller particle size decreased the packing density which is usually not the case. This phenomenon occurs due to presence of cohesion and also on the same note increase in surface energy decreases the packing density more for smaller particle than for the larger sized one. Interestingly it was found that having specific size particles in normal distribution or capping the distribution increases the packing density which is in close agreement with the work by Chen in [12].

Angle of repose which is usually used for calibration was studied and it was observed that the varying gap size or change in speed of spreading does not affect the angle of repose (AOR). Also, with addition of cohesion, the angle of repose increases. This proves the results of mass flow rate and packing density from the fact that less angle of repose (AOR) increases the fluidity of the powder.

DEM is the best available technique to analyse the powder spreading process with discrete particles. But it should be noted that the repeatability of the process may or may not give the exact same values. The reason behind this is the randomness of the particle generation and movement while spreading. Though this randomness may cause difference in values it will be considered as numerical error.

## 6.2 Recommendations for future work

This thesis bespeaks the nature of mass flow rate and packing density with respect to gap size, blade speed, COR, particle size and distribution and surface energy in the powder spreading process. This study can be furthered by adding laser sintering model with the help of EDEM™ add-on couplings with Ansys fluent which gives the capability of melting or sintering these particles. Re-coating of powder can be modeled to investigate the second layer packing density of powder. After the laser sintering or

melting process change in material properties and splattering phenomenon of particles can be studied.

Rolling friction coefficient can be added to the studied parameters to see how it affects mass flow rate and packing density. Rolling friction is responsible to restrict the rotational movement of the particles. This may result in particles not sliding from the heap giving larger values of angle of repose. In terms of numerical study different solvers such as Range-Kutta, Velocity verlet to name a few if studied may give an idea of computational accuracy of these solvers. This software package has ability to export equipment data for FEA analysis using Abaqus this can be used to perform analysis on the spreader blade for forces and temperature of the bed after the sintering/melting process. Flexible spreader blade could be tested for the spreading process which may give even more packing density and less jamming of particles for smaller gap sizes. This will be beneficial to better understand about the powder spreading process and will help improve the process.

## REFERENCES

- [1] D. Solutions, “Edem - the leading discrete element method (dem) software.” <https://www.edemsimulation.com/>.
- [2] N. S. Tannu, *A Discrete Element Approach to Predicting the Uniaxial Compressive Response of Plain Concrete*. PhD thesis, The University of North Carolina at Charlotte, 2017.
- [3] D. Goldberg and R. Mortice, Zach, “History of 3d printing: It’s older than you think,” Dec 2018.
- [4] S. Davies, “Invention, optimism realism: The back story of sls 3d printing with dr joe beaman,” Feb 2020.
- [5] H. Chen, Q. Wei, S. Wen, Z. Li, and Y. Shi, “Flow behavior of powder particles in layering process of selective laser melting: Numerical modeling and experimental verification based on discrete element method,” *International Journal of Machine Tools and Manufacture*, vol. 123, pp. 146–159, 2017.
- [6] Y. Bai, G. Wagner, and C. B. Williams, “Effect of particle size distribution on powder packing and sintering in binder jetting additive manufacturing of metals,” *Journal of Manufacturing Science and Engineering*, vol. 139, no. 8, 2017.
- [7] Q. Han, H. Gu, and R. Setchi, “Discrete element simulation of powder layer thickness in laser additive manufacturing,” *Powder Technology*, vol. 352, pp. 91–102, 2019.
- [8] P. A. Cundall and O. D. Strack, “A discrete numerical model for granular assemblies,” *geotechnique*, vol. 29, no. 1, pp. 47–65, 1979.
- [9] E. J. Parteli and T. Pöschel, “Particle-based simulation of powder application in additive manufacturing,” *Powder Technology*, vol. 288, pp. 96–102, 2016.
- [10] W. Nan, M. Pasha, T. Bonakdar, A. Lopez, U. Zafar, S. Nadimi, and M. Ghadiri, “Jamming during particle spreading in additive manufacturing,” *Powder technology*, vol. 338, pp. 253–262, 2018.
- [11] W. Nan and M. Ghadiri, “Numerical simulation of powder flow during spreading in additive manufacturing,” *Powder technology*, vol. 342, pp. 801–807, 2019.
- [12] H. Chen, Q. Wei, Y. Zhang, F. Chen, Y. Shi, and W. Yan, “Powder-spreading mechanisms in powder-bed-based additive manufacturing: Experiments and computational modeling,” *Acta Materialia*, vol. 179, pp. 158–171, 2019.
- [13] K. Mandloi, P. Amrapurkar, and H. P. Cherukuri, “Discrete element modeling of scraping process and quantification of powder bed quality for slm,” in *To be appeared in - International Manufacturing Science and Engineering Conference*, American Society of Mechanical Engineers, 2020.

- [14] J. B. Lechman and D. S. Bolintineanu, “Flowability, spreadability, and segregation.”
- [15] H. Zhu, Z. Zhou, R. Yang, and A. Yu, “Discrete particle simulation of particulate systems: theoretical developments,” *Chemical Engineering Science*, vol. 62, no. 13, pp. 3378–3396, 2007.
- [16] K. A. Buist, L. Seelen, N. Deen, J. Padding, and J. Kuipers, “On an efficient hybrid soft and hard sphere collision integration scheme for dem,” *Chemical Engineering Science*, vol. 153, pp. 363–373, 2016.
- [17] Z. Gyurkó, K. Bagi, and A. Borosnyói, “Discrete element modelling of uniaxial compression test of hardened concrete.,” *Epitoanyag-Journal of Silicate Based & Composite Materials*, vol. 66, no. 4, 2014.
- [18] C. O’Sullivan, *Particulate discrete element modelling: a geomechanics perspective*. CRC Press, 2011.
- [19] J. P. Morrissey, S. C. Thakur, and J. Ooi, “Edem contact model: adhesive elastoplastic model,” *Granul. Matter*, vol. 16, no. 3, pp. 383–400, 2014.
- [20] E. Barthel, “Adhesive elastic contacts: Jkr and more,” *Journal of Physics D: Applied Physics*, vol. 41, no. 16, p. 163001, 2008.
- [21] M. Krantz, H. Zhang, and J. Zhu, “Characterization of powder flow: Static and dynamic testing,” *Powder Technology*, vol. 194, no. 3, pp. 239–245, 2009.
- [22] M. Ghadiri, “Hardness, stiffness and toughness of particles,” *Powder Technology Handbook*, pp. 53–65, 2006.
- [23] M. A. Behjani, N. Rahmanian, A. Hassanpour, *et al.*, “An investigation on process of seeded granulation in a continuous drum granulator using dem,” *Advanced Powder Technology*, vol. 28, no. 10, pp. 2456–2464, 2017.
- [24] J. Hærvig, U. Kleinhans, C. Wieland, H. Spliethoff, A. L. Jensen, K. Sørensen, and T. J. Condra, “On the adhesive jkr contact and rolling models for reduced particle stiffness discrete element simulations,” *Powder Technology*, vol. 319, pp. 472–482, 2017.
- [25] K. Washino, E. L. Chan, and T. Tanaka, “Dem with attraction forces using reduced particle stiffness,” *Powder Technology*, vol. 325, pp. 202–208, 2018.
- [26] A. Wouterse, S. R. Williams, and A. P. Philipse, “Effect of particle shape on the density and microstructure of random packings,” *Journal of Physics: Condensed Matter*, vol. 19, no. 40, p. 406215, 2007.
- [27] R. Zou, M. Gan, and A. Yu, “Prediction of the porosity of multi-component mixtures of cohesive and non-cohesive particles,” *Chemical engineering science*, vol. 66, no. 20, pp. 4711–4721, 2011.

- [28] Z. Xiang, M. Yin, Z. Deng, X. Mei, and G. Yin, "Simulation of forming process of powder bed for additive manufacturing," *Journal of Manufacturing Science and Engineering*, vol. 138, no. 8, 2016.
- [29] E. Alizadeh, F. Bertrand, and J. Chaouki, "Comparison of dem results and lagrangian experimental data for the flow and mixing of granules in a rotating drum," *AIChE Journal*, vol. 60, no. 1, pp. 60–75, 2014.
- [30] S. Liu, Z. Zhou, R. Zou, D. Pinson, and A. Yu, "Flow characteristics and discharge rate of ellipsoidal particles in a flat bottom hopper," *Powder Technology*, vol. 253, pp. 70–79, 2014.
- [31] H. M. B. Al-Hashemi and O. S. B. Al-Amoudi, "A review on the angle of repose of granular materials," *Powder Technology*, vol. 330, pp. 397–417, 2018.
- [32] A. Mehta and G. Barker, "The dynamics of sand," *Reports on Progress in Physics*, vol. 57, no. 4, p. 383, 1994.
- [33] Y. Zhou, B. Xu, A. Yu, and P. Zulli, "Numerical investigation of the angle of repose of monosized spheres," *Physical Review E*, vol. 64, no. 2, p. 021301, 2001.